I&EC research
Industrial & Engineering Chemistry Research

pubs.acs.org/IECR

Article

Phase Equilibrium and Transport Properties of the Ionic Liquid 1-Ethyl-3-methylimidazolium Bis(trifluoromethylsulfonyl)amide and Compressed Difluoromethane and Pentafluoroethane

Karim S. Al-Barghouti, Kalin R. Baca, Mark B. Shiflett, and Aaron M. Scurto*

Cite This: *Ind. Eng. Chem. Res.* 2024, 63, 1151−1169

Read Online

ACCESS | Metrics & More | Article Recommendations | Supporting Information

ABSTRACT: Global phase behavior, high-pressure vapor−liquid equilibrium (VLE), density, viscosity, and thermal conductivity have been measured for binary mixtures of the ionic liquid (IL) 1-ethyl-3-methylimidazolium bis(trifluoromethylsulfonyl)amide ([EMIm][Tf_2N]) with either of the hydrofluorocarbon (HFC) gases, pentafluoroethane (R-125) or difluoromethane (R-32), at temperatures from 298.15 to 398.15 K and pressures to 4 MPa. At all VLE conditions investigated, R-32 is more soluble than R-125 at a given temperature and pressure. These systems are modeled with the NRTL activity coefficient model and Peng−Robinson equation of state. The mixture liquid viscosity decreases drastically with increasing compositions of dissolved gas. The thermal conductivity of both systems remains dominated by that of the IL until very high compositions of dissolved solute are achieved (>80% mol HFC). Simple mixing rules between the pure component properties can cause large, and potentially costly, errors in engineering design, as illustrated for examples in required pumping power and necessary surface area in a heat exchanger.

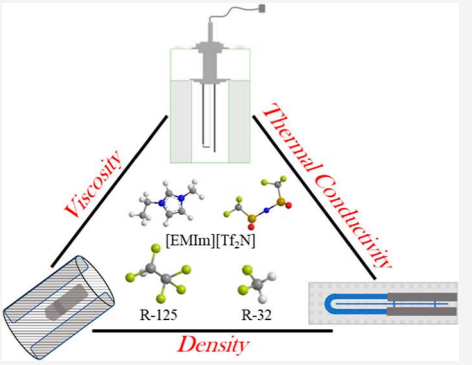

1. INTRODUCTION

The molecular tunability and unique characteristics of ionic liquids (ILs) allow for their potential use in a wide array of engineering applications. Many of the proposed applications include biphasic systems of ILs coupled with gases, for instance, in absorption refrigeration,[1−5] CO_2 capture,[6−10] lubrication for gas compression,[11,12] and gas separations among many others.[13−17] Of particular interest to this study is the proposed application of ILs in the separation of hydrofluorocarbon (HFC) gas blends. HFCs are a subset of fluorinated gases (F-gases) commonly used in refrigeration, air-conditioning, heat pumps, fire extinguishing, foam blowing, etc.[18] HFC gases are often mixed to form azeotropic or near-azeotropic blends to achieve optimal properties and applicability. Such blends include commonly used gas mixtures such as R-410A (difluoromethane (R-32) and pentafluoroethane (R-125)), R-404A (R-125, 1,1,1-trifluoroethane (R-143a), and 1,1,1,2-tetrafluoroethane (R-134a)), and R-407C (R-32, R-125, and R-134a). The ASHRAE "R-" designation is used extensively in the HFC industries.[19] Some of the HFC constituents in the aforementioned blends have elevated global warming potential and are currently subjected to legislation and regulations requiring their immediate phase out.[20−23] Alongside ILs, polymer membrane technology and porous materials have been proposed as potential agents effective in the separation of azeotropic HFC blends.[24−28]

ILs have been proposed as entrainers in extractive distillation technology to separate azeotropic or near-azeotropic HFC blends that cannot be separated using conventional distillation technology.[14,16,29−31] In extractive distillation, a solvent (here the IL) is utilized for selective absorption to allow for separation of the constituents beyond the normal azeotropic composition. The choice of an IL as an effective entrainer requires high selectivity of one component in the blend over the other(s). Hence, thermodynamic solubility data in the IL of all components present in the gas blend are needed. Furthermore, optimal design of the various unit operations involved in the separation process requires accurate knowledge of other thermodynamic properties in addition to mass, momentum, and thermal transport properties, e.g., viscosity, density, heat capacity, and thermal conductivity, of the pure IL and more importantly for the mixture of the IL and HFC component(s).

Extensive research has been carried out by various laboratory groups on the solubility of HFC gases in a multitude of ILs.[14,31−39] Shiflett and co-workers have measured the solubility of difluoromethane (R-32) and pentafluoroethane (R-125) in [EMIm][Tf_2N] using a gravimetric microbalance at three isotherms (298.15 K, 323.15 K, and 348.15 K) and

Received: October 20, 2023
Revised: December 2, 2023
Accepted: December 15, 2023
Published: January 2, 2024

https://doi.org/10.1021/acs.iecr.3c03491
Ind. Eng. Chem. Res. 2024, 63, 1151−1169

pressures up to 1.0 MPa.[40,41] The authors used a generic Redlich−Kwong equation of state (EoS) to model the VLE and vapor−liquid−liquid equilibrium (VLLE) behavior of the R-125/IL system and a variation of the NRTL model for the R-32/IL system. Both systems, with just low-moderate pressure experimental data, have been successfully modeled using the Peng−Robinson EoS with the van der Waals two-parameter mixing rule and a Boston−Mathias alpha functionality.[42]

While phase equilibrium studies are becoming more common, the mixture transport property data is far more limited in the literature. Various groups have reported on viscosities of CO_2 and IL mixtures.[43−49] Ahosseini et al. reported on the self-diffusivity and viscosity of 1,1,1,2-tetrafluoroethane (R-134a) in the IL ([HMIm][Tf_2N]) in which they show that the self-diffusivity is generally related to the viscosity of the mixture in a Stokes−Einstein relationship.[50] Density data of pure ILs is widespread in the literature at various temperatures and pressures. However, similar to mixture viscosity data, density data of ILs saturated with gases, especially HFCs, is lacking in the literature. Ren et al. report on the molar volume of various ILs saturated with R-134a.[36,37] Wang et al. report on the density and viscosity of various imidazolium ILs saturated with either difluoromethane (R-32) or pentafluoroethane (R-125) at low to moderate pressures using molecular dynamics simulations verified in part with our experimental data at 298.15 K.[51] Shiflett et al. report on molar volumes of mixtures of fluorinated gases in several different ILs at varying VLE and VLLE conditions.[41,52−55] Zhang et al. reported data on the viscosity of 1-hexy1-3-methyl-imidazolium bis(trifluoromethylsulfonyl)amide ([HMIm][Tf_2N]) saturated with hydrofluoroolefins (HFOs) *trans*-1,3,3,3-tetrafluoropropene (R-1234ze(E)) and 2,3,3,3-tetrafluoroprop-1-ene (R-1234yf) as well as [HMIm][Tf_2N] saturated with 1,1-difluoroethane (R-152a) and isobutane (R-600a).[56]

Optimization in design and sizing of heat exchangers involved in any biphasic gas/IL application requires knowledge of thermal transport properties such as thermal conductivity which is, generally through dimensionless groups, correlated with the heat-transfer coefficient. The heat-transfer coefficient, in turn, can be used to obtain the required area of heat exchange and thus the size of the heat exchanger. Various groups have measured and/or predicted thermal conductivity values of pure ILs using a variety of experimental methods and predictive methods.[57−70] We have previously reported on the thermal conductivity of [HMIm][Tf_2N] saturated with carbon dioxide.[10] Other groups have also reported on the thermal conductivity and/or thermal diffusivity (related to thermal conductivity through heat capacity and density) of ILs compressed with common gases such as carbon dioxide, helium, hydrogen, carbon monoxide, and krypton using dynamic light scattering, molecular dynamics simulations, or the transient hot-wire method.[71−73] However, we are the first group to report the thermal conductivity values of ILs 1-ethyl-3-methylimidazolium bis(trifluoromethylsulfonyl)amide [EMIm][Tf_2N] and [HMIm][Tf_2N] saturated with an HFC (R-134a).[74]

Here, we report on experimental data and modeling for the vapor−liquid equilibrium (VLE), density, and viscosity of the IL [EMIm][Tf_2N] saturated with R-32 or R-125 at 298.15 K, 323.15 K, and 348.15 K and pressures to 3.5 MPa. R-32 and R-125 constitute common azeotropic mixture R-410A and are two of the three constituents in the R-407 series of refrigerant blends. [EMIm][Tf_2N] is a commonly investigated IL with relatively moderate viscosities and is currently proposed as an entrainer for pilot-scale extractive distillation technologies for HFC separations. Experimental data are modeled with the NRTL activity coefficient model and using the Peng−Robinson EoS coupled with the van der Waals two-parameter mixing rule with a Boston−Mathias alpha functionality. In addition, thermal conductivity data of the same systems are reported herein at temperatures of 298.15, 323.15, and 348.15 K and pressures up to 3.0 MPa for R-32-saturated [EMIm]-[Tf_2N] and temperatures of 298.15, 348.15, and 398.15 K and pressures up to 4.0 MPa for R-125-saturated [EMIm][Tf_2N].

2. EXPERIMENTAL METHODS

2.1. Phase Behavior. Phase transitions and equilibria of the mixtures were assessed using a high-pressure windowed autoclave with a setup similar to that reported previously.[75] The autoclave has a volumetric capacity of ∼10 mL and includes two METAGLAS duplex borosilicate view windows rated to 40 MPa at 393.15 K. A given amount of the IL is loaded in the autoclave (∼0.5 mL) using a 1 mL microsyringe. The IL is dried in situ using a vacuum pump (∼0.007 MPa) and heating (348.15 K). The autoclave is pressurized with the gas of interest using a high-pressure *Teledyne-Isco, Inc.* 100DM syringe pump and controller. Controlled inflow of the gas is induced until the pressure reaches just below the vapor pressure of the gas at the temperature of the cell. Agitation and heating are performed using a PTFE-coated stir bar and a VWR Advanced Series ceramic-top hot/stir plate.

System pressure is monitored using a Heise ST-2H pressure Gauge equipped with an HQS-2 module capable of 10.3 MPa with a full-scale accuracy of ±0.025% (FS accuracy: 0.0026 MPa). Temperature is measured using two temperature probes placed at two different locations: the first is a type-K thermocouple (±2 K) placed in a well within the wall of the autoclave and the second is a Pt-100 resistance temperature detector (±0.1 K) immersed in the fluid. Once equilibrium is achieved, the volume expansion and number of phases observed are recorded. The system is then pressurized and allowed to equilibrate. Following equilibration, the number of phases is recorded. Regions of VLE, VLLE, and liquid−liquid equilibrium (LLE) can occur. The region of VLLE is bracketed by the lower critical end point (LCEP) and the upper critical end point (UCEP), below and above the LCEP and UCEP, respectively; only VLE exists below the vapor pressure or below the VLE mixture critical point.

2.2. Vapor−Liquid Equilibrium, Density, and Viscosity. *2.2.1. Overview: Solubility, Density, and Viscosity.* An apparatus capable of measuring high-pressure transport/thermodynamic properties and solubilities of binary systems including a low-volatility solvent is utilized to measure biphasic solubility, density, and viscosity. The apparatus is equipped with a high-pressure densimeter, high-pressure viscometer, and a high-pressure view cell. A detailed description of the constructed device is given elsewhere,[76] and an overview will be given here. The components are placed in series in an ESPEC climate-control chamber (model BTZ-475) capable of 203.15−453.15 K with an approximate ±0.2 K control. Approximately 22 mL of IL is introduced to the system and is dried under vacuum (∼0.0002 MPa) at elevated temperatures (348.15 K) for 24 h. A high-pressure (capable of 7.0 MPa) sealed vessel is pressurized with the gas of interest using

https://doi.org/10.1021/acs.iecr.3c03491
Ind. Eng. Chem. Res. 2024, 63, 1151−1169

a *Teledyne-Isco, Inc.*. 100DM syringe pump, and the mass of the pressurized refrigerant is recorded. The vessel is then used to introduce a specific mass quantity of the gas to the apparatus. To ensure that VLE equilibrium is achieved, an Eldex reciprocating piston pump (model Optos 2HM) is used to circulate the liquid by drawing the liquid from the bottom of the view cell and reintroducing it from the top after it is circulated through the components in series; this allows the liquid droplets to fall through the top of the cell and mix with the vapor phase before reentering the liquid phase. The fluid is allowed to circulate for 1 h (generally more than adequate to achieve equilibrium) at each pressure point with volumetric flow rates ranging between 5 mL/min and 30 mL/min. Pressure decay is monitored to ensure that phase equilibrium is achieved. Once equilibrium is confirmed, circulation is halted, and the fluids are allowed to settle before data is recorded. Knowledge of the mass of the IL loaded, mass of the gas introduced, density, and total system volume (including lines and components) allows for calculation of gas solubility through a mass balance method as described in detail in our previous work.[76] The temperature of the system is measured with a Pt100 RTD with an uncertainty of ±0.1 K. The pressure is measured using an OMEGA digital pressure gauge (model PX309−500AI) with an uncertainty of 0.25% full scale (±0.01 MPa). A simplified schematic of the apparatus is presented as Figure S1 in the Supporting Information.

2.2.2. Viscosity. Viscosity measurements were conducted using an oscillating piston method. The measuring device employed is a modified Cambridge Applied Systems (Currently: Cambridge Viscosity, a unit of Petroleum Analyzer Company) ViscoPro 2000, 4-SPL-440 high-pressure viscometer. The measurement principle is that of annular fluid flow around an axially oscillating piston in a cylindrical chamber.[77] Electromagnetic coils create a magnetic field that induces a force on the piston causing controlled oscillations. Two magnetic coils alternate force exertion on the piston in which one induces the force while the other determines the piston position; once the piston reaches the end of its travel distance in one direction, the magnetic coils switch functionality, and the piston is driven in the opposing direction. The oscillating movement of the piston delivers a shearing force on the fluid, and the time required for the piston to complete a travel cycle is correlated with the viscosity of the fluid. The measuring chamber is an Inconel-718 chamber with an internally mounted platinum resistance temperature detector. The cylindrical chamber slightly changes size with pressure, which results in a change in the radial distance between the piston and the cylinder walls; a correction equation and pressure-dependent adjustment parameters are provided by the manufacturer to account for this and are further developed by Duncan.[78] A detailed description of the device and the applied corrections are reported elsewhere.[76,79]

The temperature of the viscometer slightly increases when the oscillation of the piston is activated. Therefore, the viscometer is connected through its thermal jacket to an *Isotemp 3016* heated bath circulator set at 1−2 K below the desired temperature for thermal homogeneity in the measurements. The measuring system is capable of 463.15 K and 137.9 MPa with viscosities ranging from 0.2 to 10,000 mPa·s. The nominal viscosity accuracy is reported as ±1% full scale of the viscosity range of the specific piston installed. However, a run-to-run repeatability of ±0.5% is achieved in practice. Different piston sizes are used for different viscosity ranges—larger piston diameters are used for lower viscosity fluids, while smaller piston diameters are used for higher viscosity fluids. Each reported viscosity measurement is the average of 10 data points collected.

2.2.3. Density. An Anton Paar DMA HPM external measuring unit capable of pressures up to 140 MPa and temperatures up to 473.15 K was utilized for high-pressure density measurements. The fluid passed through the high-pressure vibrating U-tube oscillator and the period of oscillation is correlated with the density of the fluid. An mPDS 5 evaluation unit utilizes a conversion polynomial to correlate the oscillation period, temperature, and pressure to density.

For proper adjustments of the measurements, the coefficients of the polynomial must be accurately determined using standard samples with density ranges encompassing those of the fluid of interest. VLE equilibria is achieved as described in the previous subsections. Corrections for density due to vibrational effects, viscosity, and other influences are accounted for partially by the instrument and partially by correlation with external, independent measurements conducted using an Anton Paar DMA 5000 M densitometer. Further adjustments due to potential damping of the oscillation period caused by the viscosity of the fluid are highlighted elsewhere.[76]

The utilized temperature sensor in the densitometer has a reported uncertainty of <0.1 K. The pressure sensor coupled with the mPDS 5 unit has a reported accuracy of 0.25% full scale (FS = 3.447 MPa). The densitometer was calibrated using various standard fluids including air, *n*-octane, 1-bromobutane, degassed deionized water (15 MΩ-cm at 298.15 K), and liquid R-134a at temperatures ranging from 278.15 to 248.15 K.[80] The National Institute of Standards and Technology (NIST) REFPROP V.10.0 database[81] was used to acquire accurate density values for some of the standard fluids utilized. Density measurements have an estimated overall accuracy of ±0.15%. Further information on the aforementioned polynomial and evaluation unit operation is provided elsewhere.[80]

2.2.4. Thermal Conductivity. A *Flucon Fluid Control GmbH* thermal conductivity probe employing the transient hot-wire technique is coupled with a high-pressure equilibrium cell to measure the thermal conductivity of the biphasic IL/refrigerant mixtures. A detailed description of the system and the derivation of the governing equation are provided in our previous work,[10,74] and an overview is provided here. A transient hot-wire sensor equipped with a platinum wire is used with a high-pressure equilibrium cell that is loaded with an initial amount of IL. The system is sealed, and the IL is dried under vacuum (0.007 MPa) at 348.15 K. The vessel is heated using fiberglass-insulated heating tape connected to an in-house-built power supply controller box. The refrigerant is introduced using a *Teledyne-Isco, Inc.* 100DM syringe pump, and a PTFE-coated stir bar is used to mix the IL and refrigerant. The pressure of the system is monitored using an *OMEGA* DPG7000−3K pressure gauge with the range of 20.68 MPa (0.05% full-scale accuracy: ±0.01 MPa). Mixing is stopped once VLE is achieved, and the fluid is allowed to fully settle before measurements are taken. Equation 1 highlights the governing equation for the thermal conductivity measurements. A complete derivation of eq 1 is provided in our previous work.[10]

https://doi.org/10.1021/acs.iecr.3c03491
Ind. Eng. Chem. Res. 2024, 63, 1151−1169

Table 1. Specifications of Chemicals

Chemical Name	Chemical Structure	CAS no.	Source	Purity	Purification Method
1-Ethyl-3-methyl-imidazolium bis(trifluoromethylsulfonyl)amide ([EMIm][Tf_2N])	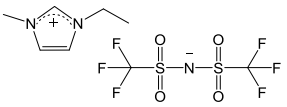	174899-82-2	IoLiTec	99+%[a]	Vacuum Drying
Pentafluoroethane (R-125)	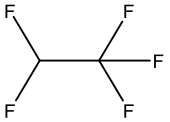	354-33-6	The Chemours Company	99+%[b]	N/A
Difluoromethane (R-32)	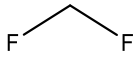	75-10-5	The Chemours Company	99.99%[b]	N/A

[a]Reported by manufacturer and confirmed here by NMR analysis after purification. [b]Specified by the supplier.

$$\lambda = \frac{Q_{t_1} + Q_{t_2}}{8\pi(T_{t_2} - T_{t_1})} \ln\frac{t_2}{t_1} \quad (1)$$

Here, λ is the thermal conductivity of the fluid, Q is the input heat per unit length, t is the time, and T is the temperature. The governing principle of the transient hot-wire method includes simplifying assumptions, e.g., infinite wire length, negligible wire heat capacity, and infinite and isotropic fluid medium.[82] These are accounted for using a one-point calibration of any fluid. Here, *n*-heptane has a reported thermal conductivity value similar to that of [EMIm][Tf_2N] at 303.15 K[81,83−87] and was used for the calibration fluid. Thermal conductivity was measured at 298.15, 323.15, and 348.15 K for the R-32-saturated [EMIm][Tf_2N] system and 298.15, 348.15, and 398.15 K for the R-125-saturated [EMIm][Tf_2N] system.

2.3. Uncertainty. *2.3.1. Solubility.* The propagation of uncertainty in measurements/calculations extends from the inherent dependencies of the method on the uncertainties of the measured loading of solvent, measured mass of gas, measured vapor and liquid densities, and the calibrated total volume of the system. It is worth noting that values such as the vapor phase gas densities are used in the calculation procedure but are not directly measured here; rather, they are obtained using rigorous equations of state defined in REFPROP and are evaluated only to the reported uncertainty.[81] The combined total uncertainty, $U_{C,\omega}$, is presented in eq 2, and a complete derivation of the point-by-point error analysis is presented in previous work.[76]

$$U_{C,\omega_1} = \sqrt{\left(\frac{\partial\omega_1(T,P)}{\partial T}\right)^2\sigma_T^2 + \left(\frac{\partial\omega_1(T,P)}{\partial P}\right)^2\sigma_P^2 + \sigma_{\omega_1}^2 + \sigma_{\omega_1,\text{repeatability}}^2} \quad (2)$$

where σ_i is the inherent error in each of the parameters presented.

2.3.2. Viscosity. For viscosity measurements along the temperatures and pressures investigated in this work, the estimated uncertainty is less than the nominal uncertainty reported by the manufacturer which is ±1% full scale of the viscosity range of the piston installed. Here, the piston utilized has a corresponding upper limit viscosity value of 50 mPa·s. Furthermore, rigorous corrections to the viscosity measurements were performed as outlined in a previous work.[76,78] Corrections for viscosity measurements are required to account for the annulus expansion of the piston chamber with temperature and pressure as well as dependency of the measured viscosity value on temperature and pressure. The combined uncertainty in viscosity measurements reported here is estimated to be 2%.

2.3.3. Density. Pure component densities for various ILs as well as simple hydrocarbons and other chemicals investigated are within good agreement with literature values (±0.5%). A complete error analysis and calibration guide is provided elsewhere.[76] A conservative estimate for uncertainty in density measurements reported in this study is ±2 kg/m^3.

2.3.4. Thermal Conductivity. The manufacturer reported uncertainty for the thermal conductivity sensor is ±1%. An independent analysis was performed, and the measurement-to-measurement precisions are found to be ±0.8 mW/m·K at 298.15 and 323.15 K, ±1.0 mW/m·K at 348.15 K, and ±2 mW/m·K at 398.15 K. The run-to-run repeatability is ±1.0 mW/m·K at 298.15, 323.15, and 348.15 K and decreases to ±1.5 mW/m·K at 398.15 K. The reported uncertainty of the calibration fluid (*n*-heptane) is approximately ±0.5 mW/m.K.[84−86,88] Therefore, the total uncertainties of the values reported here are estimated as ±1.0 mW/m K at temperatures ranging from 298.15 to 323.15 K, ±1.5 mW/m·K at 348.15 K, and ±2.5 mW/m·K at 398.15 K. Data obtained using the transient hot-wire method is often susceptible to inaccuracies due to induced convective forces which are generally expected to be most highest at higher temperatures and lower viscosities (i.e., higher gas compositions). However, no major deviations due to convection were detected in the measurements.

2.4. Chemicals. The IL, [EMIm][Tf_2N] (CAS#174899−82−2), was obtained from *Iolitec* with a manufacturer reported purity of >99%. The ILs are dried under vacuum and elevated temperatures (0.007 MPa, 348.15 K), and the water content is measured using a *Mettler Toledo C20S* Karl Fisher (KF) Coulometer prior to the measurements. Three KF measurements are conducted with masses ranging between 0.5 and 3.0 g, and the highest postdrying water content measured is less than 130 ppm. NMR analysis was conducted on the IL, and no peaks of impurity were detected. R-32 and R-125 gases were

https://doi.org/10.1021/acs.iecr.3c03491
Ind. Eng. Chem. Res. 2024, 63, 1151−1169

obtained from The Chemours Company with a reported purity of >99.9%. All chemicals used in this study and their specifications are listed in Table 1.

3. MODELING FRAMEWORK

Two different modeling approaches were attempted to correlate for the VLE. The $\gamma-\phi$ method was used with the NRTL activity coefficient model and experimental pure component data and $\phi-\phi$ was used with the Peng−Robinson EoS and a van der Waals type mixing rule.

3.1. NRTL Modeling. A general $\gamma-\phi$ formulation is used to model the VLE of both HFC/IL systems in which the nonideality of the liquid phase is represented by an activity coefficient model, and the nonideality of the vapor phase is represented by an EoS. The relevant equation is found in eq 3

$$x_i\gamma_i(T, x)P_i^{\mathrm{vap}}(T)\phi_i^{\mathrm{sat}}(T)\exp\left[\frac{\underline{V}_i^{L,\mathrm{sat}}(T)(P - P_i^{\mathrm{vap}}(T))}{RT}\right] = \phi_i^{\mathrm{V}}(T, P)P \tag{3}$$

where ϕ_i^{V} is the gas-phase fugacity coefficient of pure species i at the system temperature and pressure, P is the system pressure, x_i is the liquid-phase molar fraction of species i, γ_i is the liquid-phase activity coefficient of species i, P_i^{vap} is the vapor pressure of pure species i at the temperature of the system, ϕ_i^{sat} is the pure fugacity coefficient of species i at the system temperature at vapor−liquid saturation, and $V_i^{L\ \mathrm{sat}}$ is the molar liquid volume of species i. This assumes that the vapor phase is pure HFC gas ($y_{\mathrm{HFC}} \approx 1$), and the partial molar volume of the HFC in the liquid phase is equal to its pure component saturated molar volume, $V_i^{\mathrm{L,sat}}$, that is pressure independent. While the Poynting correction is often set to unity for low and moderate pressure systems in the literature as an assumption, it was used here as its value is often non-negligible.

The liquid-phase activity coefficient is determined using the NRTL model as follows

$$\ln\gamma_1 = x_2^2\left[\tau_{21}\left(\frac{G_{21}}{x_1 + x_2G_{21}}\right)^2 + \frac{\tau_{12}G_{12}}{(x_2 + x_1G_{12})^2}\right] \tag{4}$$

$$\ln\gamma_2 = x_1^2\left[\tau_{12}\left(\frac{G_{12}}{x_2 + x_1G_{12}}\right)^2 + \frac{\tau_{21}G_{21}}{(x_1 + x_2G_{21})^2}\right] \tag{5}$$

where G_{12} and G_{21} are defined by the following interaction parameters

$$G_{12} \equiv \exp(-\alpha\tau_{12}) \text{ and } G_{21} \equiv \exp(-\alpha\tau_{21}) \tag{6}$$

with the adjustable parameters having two temperature-dependent terms of the forms

$$\tau_{12} = \tau_{12}^{(1)} + \frac{\tau_{12}^{(2)}}{T} + \tau_{12}^{(3)}\ln(T) \text{ and } \tau_{21} = \tau_{21}^{(1)} + \frac{\tau_{21}^{(2)}}{T} + \tau_{21}^{(3)}\ln(T) \tag{7}$$

The vapor-phase fugacity, ϕ_i^{V}, and the fugacity coefficient of pure saturated HFC, ϕ_i^{sat}, as well as the molar volume, $V_i^{L,\mathrm{sat}}$, in eq 3 are obtained from ultra-accurate equations of state using REFPROP.[81,89,90] The liquid phase is assumed to be only slightly compressible, and the pure component-saturated molar volume is used in the exponential term of eq 3. The pressure term in eq 3 is iterated upon by altering the adjustable parameters $\tau_{ij}^{(1)}$,$\tau_{ij}^{(2)}$,$\tau_{ij}^{(3)}$ and the nonrandomness parameter, α, such that the error objective function between the regressed values and experimental data is minimized. Note that the nonrandomness parameter is sometimes set as a constant value of 0.2 for such gas/IL systems, but here, it is defined as a parameter of regression. The error objective function of choice is the percent average absolute relative deviation, % AARD.

3.2. EoS Modeling. The Peng−Robinson EoS coupled with a van der Waals two-parameter mixing rule (vdW-2) and the Boston−Mathias (B−M) alpha functionality was utilized to model the VLE behavior of R-32 in [EMIm][Tf_2N] as well as R-125 in [EMIm][Tf_2N].[91] Thermal conductivity measurements for the R-125/[EMIm][Tf_2N] system were conducted at temperatures ranging to 398.15 K. However, VLE data exists only at temperatures up to 348.15 K. Hence, regressed EoS parameters obtained using VLE data at 298.15, 323.15, and 348.15 K were utilized to predict VLE data at 398.15 K since **simple** (or higher order polynomial) extrapolations are expected to yield highly erroneous solubility predictions across such a vast temperature range. The Peng−Robinson EoS is combined with a two-parameter Boston−Mathias mixing rule for the attractive parameter and standard van der Waals mixing rule for the covolume parameter (vdw-BM).[91,92] The equations are as follows

$$P = \frac{RT}{\underline{V} - b_{\mathrm{m}}} - \frac{a_{\mathrm{m}}}{\underline{V}(\underline{V} + b_{\mathrm{m}}) + b_{\mathrm{m}}(\underline{V} - b_{\mathrm{m}})} \tag{8}$$

where a_{m} is the mixture attractive parameter and b_{m} is the mixture covolume parameter.

$$a_{\mathrm{m}} = \sum_{i=1}^{N}\sum_{j=1}^{N} x_ix_j\sqrt{a_ia_j}(1 - k_{ij}) + \sum_{i=1}^{N} x_i\left(\sum_{j=1}^{N} x_j\left(\sqrt{a_ia_j}\,l_{i,j}\right)^{1/3}\right)^3 \tag{9}$$

$$b_{\mathrm{m}} = \sum_{i=1}^{N} x_ib_i \tag{10}$$

with k_{ij} and l_{ij} as symmetric adjustable parameters ($k_{ij} = k_{ij}$ and $l_{ij} = l_{ij}$). The pure species parameters are

$$a_i = a_{c,i}(1 + \kappa_i(1 - \sqrt{T_{r,i}}))^2 \tag{11}$$

$$a_{c,i} = \frac{0.45724R^2T_{c,i}^2}{P_{c,i}} \tag{12}$$

$$\kappa_i = 0.37464 + 1.54226\omega_i - 0.2699\omega_i^2 \tag{13}$$

$$b_i = \frac{0.07780RT_{c,i}}{P_{c,i}} \tag{14}$$

The predicted pure IL critical properties and acentric factor were obtained from the work of Valderrama et al.[93,94] who utilized group contribution methods to predict the pure component properties. HFC properties were obtained from REFPROP.[81] The physical properties of each respective constituent are listed in Table 2.

The interaction parameters (k_{ij} and l_{ij}) were given the following temperature functionality

https://doi.org/10.1021/acs.iecr.3c03491
Ind. Eng. Chem. Res. 2024, 63, 1151−1169

Table 2. Physical Properties of [EMIm][Tf_2N], R-32, and R-125[a]

component	MW	T_b/K	T_c/K	P_c/bar	ω
[EMIm][Tf_2N]	391.3	816.7	1249.3	32.7	0.2157
R-125	120.02	225.06	339.17	36.2	0.3052
R-32	52.024	221.50	351.26	57.82	0.2769

[a]IL parameters from ref 93 and R-125 and R-32 parameters from ref 81.

$$k_{ij} = k_{ij}^{(1)} + k_{ij}^{(2)}T + \frac{k_{ij}^{(3)}}{T} \tag{15}$$

$$l_{ij} = l_{ij}^{(1)} + l_{ij}^{(2)}T + \frac{l_{ij}^{(3)}}{T} \tag{16}$$

ASPEN Plus V10 (thermodynamics package) was utilized with a Maximum likelihood objective function to regress the data and obtain elements of the k_{ij} and l_{ij} parameters. The k_{ij} and l_{ij} elements obtained were then used to extrapolate VLE behavior to 398.15 K (for R-125/[EMIm][Tf_2N]).

3.3. Henry's Law Constant Predictions. Henry's constants were calculated for the R-125/[EMIm][Tf_2N] system at the temperatures with available experimental solubility data. The obtained Henry's constants with temperature were used to predict a Henry's constant at 398.15 K to obtain solubility at the conditions of the other measurements.

At low to moderate pressures (compositions), the infinite-dilution-based activity coefficient, γ_i*, can be neglected, and the *Poynting-like* correction is assumed to be unity. Furthermore, the mixture liquid fugacity of the solute can be linearly correlated with the solute's molar composition in the liquid phase and Henry's constant as the slope. The mixture liquid fugacity of the solute is also equal to the pure component vapor-phase fugacity as shown in eq 17.

$$\overline{f}_i^{L}(T, x) = H_i(T)x_i = f_i^{V}(T, P) \tag{17}$$

Vapor-phase fugacity of R-125 was obtained from REFPROP.[81] The slope of the linear portion of the equilibrium vapor-phase fugacity versus the experimental solute mole fraction plot would yield the Henry's law constant. Henry's constant[95] has a temperature dependence that can be correlated with the infinite-dilution partial molar enthalpy ($\overline{\Delta_{sol}H_i^{\infty}}$) of solution.

$$\frac{\overline{\Delta_{sol}H_i^{\infty}}}{R} = \left(\frac{\partial \ln H_i}{\partial\left(\frac{1}{T}\right)}\right)_P \tag{18}$$

The infinite-dilution partial molar enthalpy of solution is only expected to vary slightly with temperature in the range considered and is assumed to be constant. Equation 18 can be integrated to extrapolate Henry's constant to higher temperatures, T_2 = 398.15 K.

$$\frac{H_i(T_2)}{H_i(T_1)} \approx \exp\left[\left(\frac{\overline{\Delta_{sol}H_i^{\infty}}}{R}\right)\left(\frac{1}{T_2} - \frac{1}{T_1}\right)\right] \tag{19}$$

The extrapolated Henry's constant at 398.15 K was then used to predict solubility at that temperature.

4. RESULTS AND DISCUSSION

4.1. Phase Behavior, Vapor Liquid Equilibrium, and Modeling. *4.1.1. Phase Behavior.* Most IL/HFC mixtures are characterized as Type V systems according to the Scott-van Konynenburg phase-behavior scheme.[36] Type V systems exhibit a LCEP in which, below that temperature and below the saturation pressure of the more volatile substance, VLE exists. While at and above the saturation pressure of the more volatile substance, a single miscible liquid layer forms. At temperatures above the LCEP but below the UCEP, VLE,

Table 3. Pressure, HFC Composition, Mass Density, Dynamic Viscosity, and Kinematic Viscosity of R-32-Saturated [EMIm][Tf_2N] and R-125-Saturated [EMIm][Tf_2N][a]

R-125/[EMIm][Tf_2N]								R-32/[EMIm][Tf_2N]						
T [K]	P [MPa]	$x_{R\text{-}125}$	σ_x	$U_{c,\,x_{R\text{-}125}}$	ρ [kg/m^3]	η mPa·s	ν^c cSt	P [MPa]	$x_{R\text{-}32}$	σ_x	$U_{c,\,x_{R\text{-}32}}$	ρ [kg/m^3]	η mPa·s	ν^c cSt
298.15	[b]	0.000	0.000	0.000	1516	31.8	21.0	[b]	0.00	0.000	0.00	1517	31.4	20.7
	0.099	0.055	0.007	0.009	1515	27.3	18.0	0.232	0.21	0.009	0.02	1502	17.5	11.6
	0.300	0.158	0.005	0.009	1514	21.5	14.2	0.505	0.39	0.005	0.02	1481	8.2	5.5
	0.605	0.312	0.004	0.008	1511	14.8	9.8	0.701	0.49	0.003	0.02	1463	6.4	4.4
	0.801	0.407	0.003	0.007	1508	11.0	7.3	0.878	0.58	0.002	0.02	1445	4.0	2.8
								1.269	0.74	0.001	0.01	1389	1.8	1.3
323.15	[b]	0.000	0.000	0.000	1492	15.9	10.7	[b]	0.00	0.000	0.00	1492	15.8	10.6
	0.286	0.079	0.007	0.008	1491	13.5	9.1	0.493	0.23	0.010	0.02	1472	9.0	6.1
	0.444	0.122	0.006	0.008	1490	12.5	8.4	0.756	0.33	0.007	0.01	1461	7.2	4.9
	0.860	0.230	0.005	0.007	1487	9.8	6.6	1.211	0.46	0.004	0.01	1437	4.6	3.2
	1.679	0.425	0.004	0.007	1478	6.1	4.1	1.758	0.60	0.003	0.01	1401	2.7	1.9
	2.354	0.571	0.004	0.008	1464	4.5	3.1	2.667	0.79	0.001	0.02	1291	1.2	0.9
348.15	[b]	0.000	0.000	0.000	1467	9.0	6.1	[b]	0.00	0.000	0.00	1468	8.6	5.8
	0.250	0.043	0.006	0.008	1466	8.4	5.8	0.326	0.11	0.012	0.02	1458	7.0	4.8
	0.613	0.105	0.006	0.008	1465	7.7	5.2	0.655	0.21	0.009	0.02	1450	5.9	4.1
	1.315	0.222	0.005	0.008	1462	6.5	4.4	1.248	0.35	0.006	0.02	1432	4.2	3.0
	2.283	0.359	0.003	0.008	1455	5.3	3.6	2.302	0.53	0.003	0.02	1396	2.5	1.8
	3.137	0.46	0.002	0.01	1449	4.6	3.2	3.652	0.70	0.002	0.02	1334	1.5	1.1

[a]Reported standard uncertainties: $u(T)$ = 0.1 K; $u(P)$ = 0.01 MPa; $u(x)$ = 0.01; $u(\rho)$ = 2 kg/m^3; $u(\eta)$ = 0.3 mPa·s. [b]Pure IL at ambient pressure (gauge). [c]ν = kinematic viscosity.

https://doi.org/10.1021/acs.iecr.3c03491
Ind. Eng. Chem. Res. 2024, 63, 1151−1169

VLLE, LLE, or mixture critical points ($L = L$ and $V = L$) are possible. VLE exists at all conditions above the UCEP and below the mixture critical point.

Experimental phase behavior studies and NRTL modeling predictions conducted previously by Shiflett and Yokozeki[41] indicate regions of VLLE and LLE for the system of R-125/[EMIm][Tf_2N] at pressures at and above the vapor pressure of pure R-125 and at all temperatures between the LCEP and UCEP. The LCEP was experimentally determined to be ~270 K. In our study, the findings are confirmed through both modeling techniques used as well as experimental observation utilizing the high-pressure view cell described in Section 2.1. The UCEP is observed at the same temperature and pressure, within experimental accuracy, as the pure component critical point of R-125 (339.17 K, 3.61 MPa).

Interestingly, the R-32/IL system actually exhibited liquid−liquid (LLE) and VLLE. A LCEP was observed at ~337 K and terminating at the UCEP, which is approximately the same as the pure R-32 critical point (351.26 K, 5.78 MPa). The PR−BM−vdW−2 model utilized in this study predicts a LCEP of 336 K for the R-32/IL system which is remarkably close to the experimentally obtained value of ~337 K. The EoS accurately predicts the pressure at which the liquid partitioning occurs for the R-32/IL system at 348.15 K of 5.38 MPa compared to the experimental value of 5.4 MPa. The difference between the two values is less than the uncertainty of the experimental method employed. The previous studies of this R-32/[EMIm][Tf_2N] system were conducted by Shiflett and Yokozeki,[30,40] and they only observed VLE. However, their experimental measurements only went to temperatures 348.05 K and pressures 1.0 MPa and they only extrapolated their models to 1.4 and 4.0 MPa.

Mixture critical points ($L = L$ or $V = L$) for either R-32 or R-125 with the IL were not encountered at the moderate pressures investigated here but are still believed to occur at higher pressures according to the Type V behavior. The R-125/IL system was investigated at 343.15 K to a pressure of 23 MPa, and only VLE was observed. The R-32/IL system maintains VLE to a maximum investigated pressure of 15 MPa at 343.15 K. Other IL/HFC systems in the literature exhibit mixture critical points at elevated pressures (>8 MPa above the critical temperature).[37,75] All mixture data points reported in this study for density, viscosity, and thermal conductivity were conducted solely in the VLE regime.

4.1.2. Solubility. The VLE solubility data measured in this study are presented in Table 3 and plotted in Figures 1 and 2. In the figures, error bars at each data (see Table 3) point are generally within the size of the symbols themselves and are omitted from the plots. For the R-32/IL system, the solubility exhibits a relatively linear increase with pressure at 298.15 K (to 80% mol_{HFC}). The linearity of the composition versus pressure relationship decreases with increasing temperature. At 323.15 K, the trend is relatively linear to an HFC mole fraction of 0.6 and becomes more nonlinear at high compositions. Similarly, the 348.15 K isotherm has a relatively linear trend until approximately a mole fraction composition of R-32 of about 0.4. The data for the R-125/IL system is limited to a low-to-moderate composition regime. The three isotherms for the R-125/IL system exhibit highly linear increases in composition with increasing pressure throughout the measured pressure (composition) range. The linearity decreases slightly with increasing temperature. The modeling techniques employed predict drastic deviations from linearity at higher

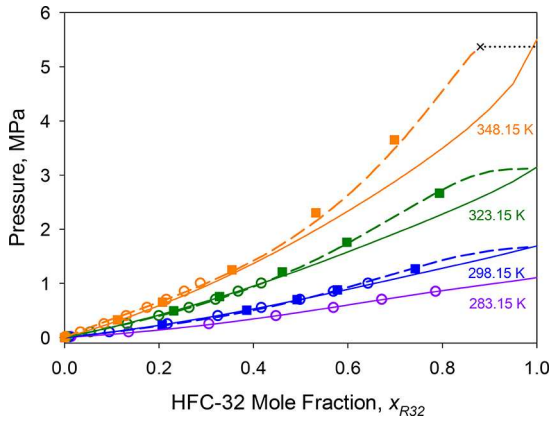

Figure 1. Solubility data for R-32 in [EMIm][Tf_2N]. Experimental data (■), literature data from Shiflett et al.[40] (○), data from Sosa et al.[38] (+) at 303.15 K, and data from Sousa et al.[39] (△) at 0.101 MPa and temperatures between 288.11 and 308.19 K. Solid lines represent the NRTL activity coefficient model, and dashed lines represent the Peng−Robinson EoS (BM−vdW−2) predictions. (*X*) Represents the start of the EoS-predicted VLLE region.

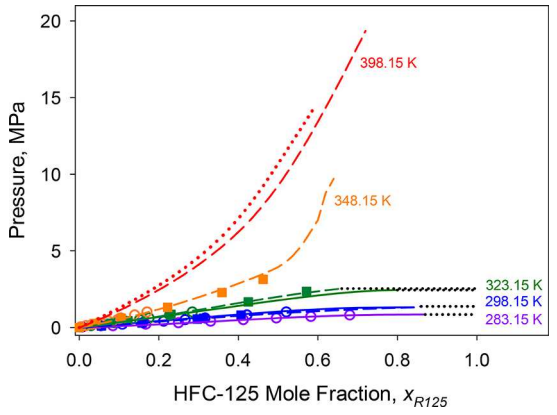

Figure 2. Solubility data for R-125 in [EMIm][Tf_2N]. Experimental data (■), literature data from Shiflett et al.[41] (○), and data from Sosa et al.[38] (+) at 303.15 K. Solid lines represent the NRTL activity coefficient model, dashed lines represent the Peng−Robinson EoS (BM−vdW−2) predictions, and dotted red line represents Henry's law model. Dotted black lines are predicted VLLE regions.

compositions as VLLE and supercritical regimes are approached. Several of the lower pressure data (<1 MPa) overlap with the measurements of Shiflett and Yokozeki using a gravimetric microbalance method.[40,41] By interpolating this lower pressure data, our measurements for R-125 in [EMIm]-[Tf_2N] have a total percent-average relative deviation (% AARD) of ~2.7% for the three isotherms from their data. For the overlapping data for the R-32/[EMIm][Tf_2N] system, the % AARD is ~2.0% for the three isotherms. The acquisition of density and solubility data simultaneously allows for the presentation of the composition in different solubility units. Tables S1 and S2 include the molality ($mol_{gas}/kg_{solvent}$), molarity ($mol_{gas}/liter_{solution}$), weigh fractions, volume expansions, and their respective point-by-point errors.

4.1.3. NRTL Modeling. The NRTL model well correlates the experimental solubility data with an overall % AARD of less than 7% for both systems. The binary interaction parameters that were regressed for R-32 with [EMIm][Tf_2N] and R-125 with [EMIm][Tf_2N] can be found in Table 4. It is important to note that the data sets used for the NRTL regression were a

https://doi.org/10.1021/acs.iecr.3c03491
Ind. Eng. Chem. Res. 2024, 63, 1151−1169

Table 4. NRTL Activity Coefficient Model Binary Interaction Parameters

HFC (1) + IL (2)	$\tau_{12}^{(1)}$	$\tau_{12}^{(2)}$ (K)	$\tau_{12}^{(3)}$ (K^{-1})	$\tau_{12}^{(1)}$	$\tau_{12}^{(2)}$ (K)	$\tau_{12}^{(3)}$ (K^{-1})	α
R-32 + [EMIm][Tf_2N]	-9.49×10^{-1}	9.59×10^{2}	1.06×10^{-1}	−3.25	-6.21×10^{2}	5.96×10^{-2}	0.200
R-125 + [EMIm][Tf_2N]	−5.68	-1.30×10^{-1}	1.64	-1.30×10^{1}	−4.06	2.08	0.200

combined set of the experimental data from this study and data reported previously at generally lower pressures.[40] The $\gamma-\phi$ NRTL method is used only for isotherms that fall below the critical temperature of each respective HFC. The % AARD for the regression of each system is reported in Table 5. The

Table 5. % AARD for the NRTL Activity Coefficient Model Relative to Experimental Data

temperature	R-32 (1) + IL (2)	R-125 (1) + IL (2)
283.15	6.7	10.68
298.15	1.7	1.3
323.15	5.0	3.3
348.15	6.7	

highest % AARD for both systems is observed at the lowest reported isotherm, 283.15 K. Beyond the linear Henry's regime, the highest deviation is observed at the highest pressure data points at 348.15 K for the R-32/IL system and 323.15 K in both systems and is likely due to the approaching onset of VLLE and LLE regions. Better regression fits may be achieved by regressing the data at each individual isotherm in contrast to the entirety of the data as done here. A sensitivity analysis of the interaction parameters is presented in Figure S2 of the Supporting Information.

4.1.4. Peng−Robinson EoS and vdW-2 Mixing Rule. The lower pressure experimental VLE data sets reported by Shiflett and Yokozeki[40,41] are combined with higher pressure VLE data measured in this study to form a single, comprehensive experimental data set. The Peng−Robinson EoS with Boston−Mathias and van der Waals mixing rule well correlate experimental data for both systems as illustrated in Figures 1 and 2. The overall % AARD for the EoS relative to the experimental data is 6.5% for R-125/[EMIm][Tf_2N] with the highest deviation occurring at 348.15 K. Similarly, the overall % AARD for the R-32/[EMIm][Tf_2N] system is 4.0% with the highest deviation occurring at 348.15 K. The % AARD for the respective isotherms are reported in Table 7 for both systems. It is worth noting that the R-125/[EMIm][Tf_2N] system exhibits relatively high deviations at the first three pressure points at 348.15 K, which if omitted, the % AARD improves to 8.4%. The regressed parameters of the Peng−Robinson EoS and vdW-2 mixing rule with a B−M alpha functionality are reported in Table 6.

The EoS/mixing rule parameters regressed using data at 298.15, 323.15, and 348.15 K were used to predict solubility at 398.15 K for the R-125/[EMIm][Tf_2N] system. The predicted solubility with pressure at 398.15 K is illustrated in Figure 2. The extrapolated solubility at higher temperatures is used to correlate measured pressure at elevated temperatures to composition in the thermal conductivity experiments since

Table 7. % AARD for the PR−BM−vdW−2 EoS Regression Relative to Experimental Data

temperature	HFC-32 (1) + IL (2)	HFC-125 (1) + IL (2)
298.15	2.37	1.54
323.15	1.81	5.45
348.15	8.50	11.20

solubility data at elevated temperatures are not available and cannot be readily obtained with the current system configuration. The % AARD between the values predicted at 398.15 K using the EoS/mixing rule compared to those obtained using a Henry's constant model is 8.1%.

The NRTL model and Peng−Robinson−BM−vdW model utilized in this study are able to successfully predict the existence of VLLE and LLE regions at the temperatures investigated here between the LCEP and UCEP mentioned above for the R-125/[EMIm][Tf_2N] system at and above the saturation pressure of R-125 (within experimental accuracy). However, only the Peng−Robinson EoS with the BM−vdW−2 mixing rule is able to predict a VLLE and LLE partitioning for the R-32/[EMIm][Tf_2N] system.

4.2. Density/Molar Volume and Excess Molar Volume. The measured mass densities for the R-32/[EMIm][Tf_2N] system at the three temperatures investigated in this study are illustrated in Figure 3 and those of R-125/

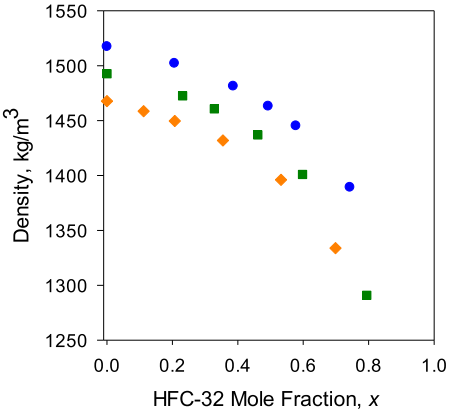

Figure 3. Liquid-phase mass density of R-32/[EMIm][Tf_2N] with molar composition of dissolved R-32. (Blue ●) 298.15 K, (green ■) 323.15 K, and (orange ♦) 348.15 K.

[EMIm][Tf_2N] are illustrated in Figure 4. The experimental data for both systems are reported in Table 3. For many experiments in the literature, the density is measured in a separate experiment by equilibrating the vapor and liquid at a given temperature and pressure and then using external VLE

Table 6. PR−BM−vdW−2 EoS Regressed Parameters

HFC (1) + IL (2)	$l_{12}^{(1)}$	$l_{12}^{(2)}$ (K)	$l_{12}^{(3)}$ (1/K)	$k_{12}^{(1)}$	$k_{12}^{(2)}$ (K)	$k_{12}^{(3)}$ (1/K)
HFC-32 + [EMIm][Tf_2N]	14.744	−0.0238	−2286.9	3.32880	−0.0055	−520.71
HFC-125 + [EMIm][Tf_2N]	4.4238	−0.0063	−747.83	1.4618	−0.0023	−239.81

https://doi.org/10.1021/acs.iecr.3c03491
Ind. Eng. Chem. Res. 2024, 63, 1151−1169

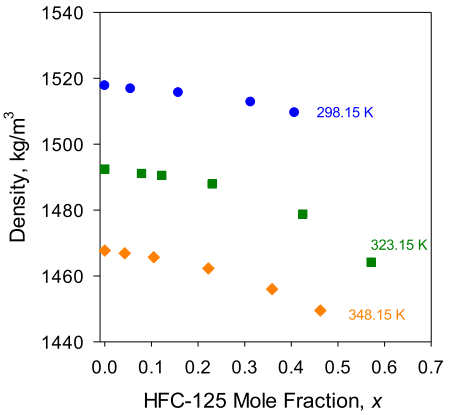

Figure 4. Liquid-phase mass density of R-125/[EMIm][Tf_2N] with molar composition of dissolved R-125. (Blue ●) 298.15 K, (green ■) 323.15 K, and (orange ♦) 348.15 K.

composition data to interpolate the compositions at the temperature and pressure of the density experiments. However, here the density and equilibrium liquid composition are measured simultaneously. Both systems exhibit a gradual decrease in mass density with increasing pressure (refrigerant composition) along the composition regimes investigated. The R-32/[EMIm][Tf_2N] system exhibits a pronounced decrease in mass density with increasing HFC composition. A 4−6% decrease in density is observed for the R-32/[EMIm][Tf_2N] system at the three temperatures investigated and a molar composition of ∼0.50. It is worth noting that the pure saturated liquid density of R-32 at 298.15 and 323.15 K is 961 and 839.3 kg/m^3, respectively, while the saturated liquid density of R-125 at the same temperatures is 1189 kg/m^3 and 1001 kg/m^3.[81,89,90] Only a slight decrease in density is observed in the R-125/[EMIm][Tf_2N] system with increasing HFC composition as the greatest decrease in density does not exceed 1% along the composition and temperature ranges investigated. It is expected that hydrostatic pressure effects along the pressure regimes investigated have only a slight effect on the mixture density except, perhaps, at the highest compositions of the dissolved gas.

The Peng−Robinson (BM−vdW−2) model does an adequate job at predicting the molar volume of the systems at a given condition as illustrated in Figures 5 and 6. The model has a % AARD of less than 5% compared to experimental data measured here. However, the model has a negative bias (underprediction) across all isotherms investigated. This results in an overprediction for the density (*kg/m*^{3}), and the model actually predicts a maximum in density for all of the isotherms at approximately a mole fraction of HFC of 0.6.

The excess molar volume, $\underline{V}^{EX}$, for both systems is calculated as shown in eq 21.

$$\underline{V}^{EX} = \underline{V}_m(T, P, x) - [x_{IL}\underline{V}_{IL}(T, P) + x_{HFC}\underline{V}_{HFC}(T, P)] \quad (20)$$

where $\underline{V}^{EX}$ is the excess molar volume, $\underline{V}$ is the mixture molar volume, and $\underline{V}_i$ is the molar volume of each respective pure component. The required pure liquid molar volumes for the HFC at the same temperature and pressure of the system would not be available, as they would be gases at the system pressure. To overcome this, the saturated liquid molar volumes at their respective vapor pressure are adjusted to the mixture

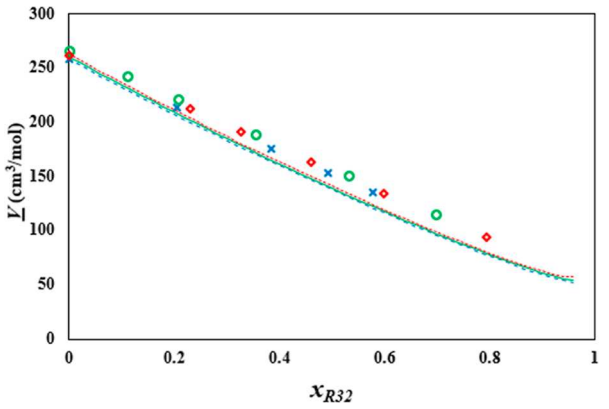

Figure 5. Liquid-phase molar volume of R-32/[EMIm][Tf_2N] with molar composition of dissolved R-32. Markers are experimental data points—(x) 298.15 K, (○) 323.15 K, and (◊) 348.15 K. Lines are EoS predictions—blue = 298.15 K, green = 323.15 K, and red = 348.15 K.

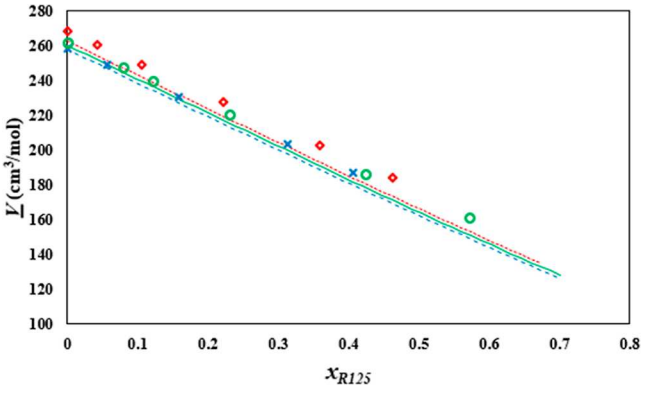

Figure 6. Liquid-phase molar volume of R-125/[EMIm][Tf_2N] with molar composition of dissolved R-125. Markers are experimental data points—(x) 298.15 K, (○) 323.15 K, and (◊) 348.15 K. Lines are EoS predictions—blue = 298.15 K, green = 323.15 K, and red = 348.15 K.

pressure by extrapolating the liquid molar volume at the same temperature to pressures below the vapor pressure. This results in a relatively small correction over the saturated molar volume at the vapor pressure, but as the excess molar volume at low compositions is relatively small, it was deemed necessary. The analysis was limited to 298.15 and 323.15 K since the elevated isotherms investigated in this study are beyond the critical temperature of pure component R-125. The excess molar volumes for both systems are illustrated in Figure 7.

Within uncertainties of the measurements and those of the pure component data reported (and adjusted), the excess molar volumes of both systems are negative and have relatively similar magnitudes. However, R-125/[EMIm][Tf_2N] exhibits a slightly larger negative excess molar volume at a given composition at the two temperatures; this is a similar observation as found previously for R-125 and R-32 in various imidazolium-based ILs.[51] Interestingly, the absolute excess molar volume of R-125/[EMIm][Tf_2N] slightly decreases with increasing temperature, while that of R-32/[EMIm][Tf_2N] increases with increasing temperature. Data reported by Makino et al.[96] on the density of [EMIm][Tf_2N] and CO_2 mixtures was used to calculate excess molar volumes for the same system. The CO_2/[EMIm][Tf_2N] system behaves similar

https://doi.org/10.1021/acs.iecr.3c03491
Ind. Eng. Chem. Res. 2024, 63, 1151−1169

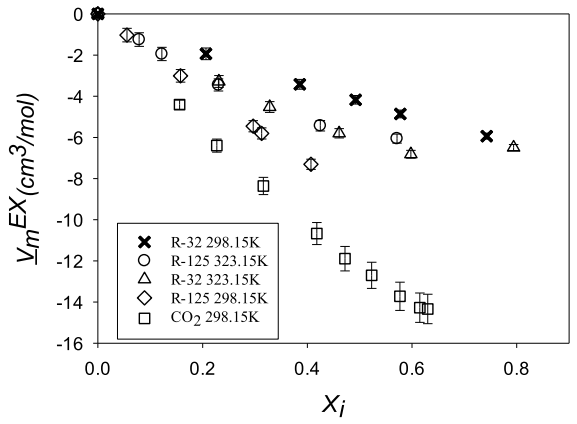

Figure 7. Excess molar volume of R-32/[EMIm][Tf_2N] at 298.15 K (X); R-125/[EMIm][Tf_2N] at 298.15 K (◊); R-32/[EMIm][Tf_2N] at 323.15 K (Δ); R-125/[EMIm][Tf_2N] at 323.15 K (○), and CO_2/[EMIm][Tf_2N] data at 298.15 K (□) from Makino et al.[96]

to the R-32/[EMIm][Tf_2N] and R-125/[EMIm][Tf_2N] systems in which a negative excess molar volume is exhibited along the composition ranges reported. However, the CO_2/IL system exhibits a larger absolute excess molar volume than either of the HFC/IL systems investigated in this study.

Only R-32 observes a minimum in excess molar volume within the composition regimes investigated/reported. Here, the R-32 system exhibits a minimum at a R-32 molar composition of ∼0.60 (observed at 323.15 K). Due to the limited data available at higher dissolved gas compositions, it cannot be concluded exactly where the other systems form minima along elevated composition regimes. Nevertheless, it is worth noting that all of the aforementioned systems exhibit higher magnitudes of excess molar volumes than typical organic liquid mixtures.[97,98] Moreover, systems involving 2,2,2-trifluoroethanol (TFE) or methanol and imidazolium-based ILs exhibit excess molar volumes that are 10−100X less than those of the HFC/IL systems investigated here.[99,100] In addition, water/IL mixtures typically display much lower magnitudes of excess molar volumes (compared to systems in this study).[101]

The negative excess molar volumes may indicate free volume effects and/or stronger intermolecular attractive interactions between the two components in the mixture relative to those present in the pure components. HFCs presented in this study have larger dipole moments and dielectric constants than CO_2 and possess the potential for hydrogen bonding.[102] The dipole moment of R-32 is 1.978 D and that of R-125 is 1.563 D.[33] The dielectric constant of R-32 and R-125 as saturated liquids at 298.15 K are 14.7 and 5.1, respectively.[103] Yet, the excess molar volumes of the HFC/IL systems more closely resemble that of CO_2/IL systems, where CO_2 has zero dipole moment and a very low dielectric constant rather than water/IL systems where it is believed that the ions can be solvated and dissociated. The method of McGowan was used here to estimate the molecular volumes of the HFC gases—R-32 has an estimated molecular volume of 28.49 cm^3/mol, and R-125 has an estimated molecular volume of 47.89 cm^3/mol based on their constituent atomic volumes and bond designations.[104] Applying the analysis of Klähn et al.,[105] it can be reasoned that unperturbed [EMIm][Tf_2N] would lack a significant number of cavity sites (potentially not any) with size large enough to accommodate the HFCs. This would indicate potential ion reorientations rather than drastic expansions similar to phenomena hypothesized in CO_2 dissolution processes.[106] Furthermore, MD studies of Wang et al. demonstrate that the cation−cation, anion−anion, and cation−anion radial distribution functions of similar imidazolium-based ILs are generally unaffected by the addition of R-32 and/or R-125 (probed to molar compositions up to ∼60%$_{HFC}$)—a similar phenomenon as observed in many CO_2/IL systems.[51] This may indicate that the HFCs might be interacting with the ILs but are not able to fully disrupt the ion−counterion interactions to appreciable extents as observed in the one-phase IL/water systems.

4.3. Viscosity. Experimental liquid-phase dynamic viscosity measurements were conducted for saturated (VLE) mixtures of R-32/[EMIm][Tf_2N] and R-125/[EMIm][Tf_2N], and the results are reported in Table 3 and illustrated in Figure 8 for R-32/[EMIm][Tf_2N] and Figure 9 for R-125/[EMIm][Tf_2N]. The decrease in viscosity for both systems has a relatively linear trend throughout the composition regimes investigated, at least until ∼40% mol of the dissolved HFC. The highest deviation from linearity is observed at the 298.15 K isotherm for the R-32/[EMIm][Tf_2N] system. Again, these systems are in VLE at a specific pressure. The decrease appears to largely be a "dilution" effect of adding a component with orders of

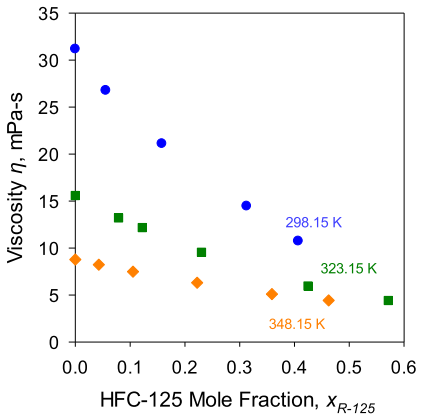

Figure 8. Liquid-phase viscosity of R-32/[EMIm][Tf_2N] with various compositions of dissolved R-32. (Blue ●) 298.15 K, (green ■) 323.15 K, and (orange ♦) 348.15 K.

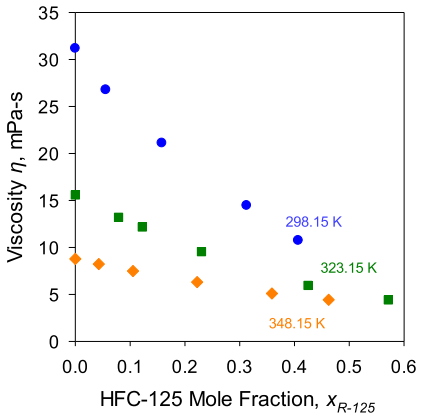

Figure 9. Liquid-phase viscosity of R-125/[EMIm][Tf_2N] with various compositions of dissolved R-125. (Blue ●) 298.15 K, (green ■) 323.15 K, and (orange ♦) 348.15 K.

https://doi.org/10.1021/acs.iecr.3c03491
Ind. Eng. Chem. Res. 2024, 63, 1151−1169

magnitude lower viscosity as a pure saturated liquid. For instance, the viscosity of saturated liquids R-32 and R-125 at 298.15 K is 0.11 mPa.s and 0.14, and 0.083 mPa.s and 0.089 at 323.15 K, respectively. For comparison, the viscosity of pure [EMIm][Tf_2N] is 31 mPa.s at 298.15 K and 16 at 323.15 K.

Both systems exhibit a large decrease in dynamic viscosity with increasing dissolved gas composition. The decrease in viscosity relative to the pure component IL viscosity at a given composition is nearly identical for both systems; that is, both HFCs have similar effects on the viscosity decrease with composition of dissolved gas especially at lower compositions (e.g., <40% mol). The percent decrease in viscosities versus the pure IL viscosity with increasing dissolved HFC composition for both systems at the various isotherms investigated are illustrated in Figure S3. Viscosity reductions versus the pure IL reached as high as 90+% for the [EMIm][Tf_2N] and R-32 system at 298.15 K and ∼74% mol R-32 (∼1.27 MPa). As shown, a similar effect at a given composition and temperature indicates that the gases have a general and nonspecific diluent effect on the viscosity of the liquid phase especially at lower compositions. This indicates that the diluent effect in the low-composition regime is almost a colligative property. However, at higher compositions, R-32 has a higher viscosity reduction at a given mole fraction composition. Pure saturated liquid R-32 has a lower viscosity than R-125, i.e., −20% at 298.15 K. Thus, dissolved in the IL, R-32 has a higher viscosity reduction at a given composition, which occurs at a higher pressure than in the R-125 system. From the VLE data, a higher pressure is required to achieve this composition for the R-32 system versus the R-125 system. However, a hydrostatic effect in this pressure range is not believed to affect the observed behavior of the mixture viscosity to any noticeable effect.

In collaboration with Maginn and co-workers, we have recently reported on the viscosity of IL 1-butyl-3-methyl-imidazolium tetrafluoroborate ([BMIm][BF_4]) and HFC gases R-32 and R-125 at 298.15 K.[51] Both [BMIm][BF_4] systems investigated exhibit steeper decreases in viscosity with increasing dissolved gas composition relative to the [EMIm]-[Tf_2N] systems investigated in this study. We have also measured the viscosity of [RMIm][Tf_2N] ILs saturated with CO_2 or R-134a.[43,50] The measured viscosities as a function of dissolved gas composition for the IL systems exhibit similar trends as those for the HFC/IL systems measured here.

Several studies have been conducted by our group, as well as others, on the viscosity of IL 1-hexy1-3-methyl-imidazolium bis(trifluoromethylsulfonyl)amide ([HMIm][Tf_2N]) saturated with either HFC gases or HFO (hydrofluoroolefins) gases. Zhang et al. report on the viscosity of IL [HMIm][Tf_2N] saturated with HFC gas 1,1-difluoroethane (R-152a) as well as [HMIm][Tf_2N] saturated with hydrofluoroolefins *trans*-1,3,3,3-tetrafluoropropene (R-1234ze(E)) and 2,3,3,3-tetrafluoroprop-1-ene (R-1234yf) at temperatures ranging between 283.15 and 343.15 K.[56,107] The decrease in viscosity with increasing dissolved gas composition exhibited by all HFC/or HFO/[RMIm][Tf_2N] systems is similar within the limits of uncertainty.

To compare the mixture viscosity values for the different systems in relation to their respective idealized mixture viscosities, "excess" viscosities were calculated as shown in eq 21.

$$\eta^{EX}(T, P, x) \approx \eta^{EX}(T, x) = \eta_m(T, x) - [x_{IL}\eta_{IL}(T, P) + x_{HFC}\eta_{HFC}(T, P)] \quad (21)$$

where η^{EX} is the "excess" viscosity, η_m is the measured mixture viscosity, and $\eta_i(T,P)$ is the pure component viscosity in the liquid phase at the respective temperature and pressure. "Excess viscosity" is not regarded as a true excess property in the equilibrium thermodynamic sense but is rather utilized here to merely compare the measured real system viscosities to those of an idealized solution. For the HFCs and CO_2, the viscosity at the saturation temperature with an added pressure dependency based on the extrapolated isothermal pressure−viscosity relation, in an analogous manner to excess molar volume, is applied for increased accuracy. Both HFC/[EMIm][Tf_2N] systems investigated here as well as the CO_2/[EMIm][Tf_2N] system investigated previously exhibit a negative "excess" viscosity along the pressure regimes investigated. At 298.15 K, the magnitude of the "excess" viscosity for the HFC/IL systems is greater than that of the CO_2/IL system. Furthermore, both HFC/IL systems exhibit a decrease in the absolute "excess" viscosity with increasing temperature. At both isotherms examined (298.15 and 323.15 K), the R-32/IL mixture has a larger magnitude of "excess" viscosity than the R-125/IL system. The relatively high dielectric constant of R-32 compared to CO_2 and R-125 may potentially allow it to form stronger interactions with the IL and may possibly contribute to partial solvation of the ions, leading to an evidently larger (negative) viscosity deviation from ideality. The dielectric constant of saturated liquid R-32 at 298.15 K is 14.7, and those of R-125 and CO_2 are 5.1 and 1.4, respectively (CO_2 reported at 299 K).[103,108]

Figure 10 illustrates the negative "excess" viscosity trends for the systems investigated here and the CO_2/[EMIm][Tf_2N] system. Moreover, Ahosseini et al. have shown that the "excess" viscosity of R-134a-saturated [HMIm][Tf_2N] is positive for three isotherms (298.15 K, 323.15 K, and 343.15 K) and decreases with increasing temperature.[50] Yet, CO_2/[HMIm][Tf_2N] investigated previously exhibits a negative

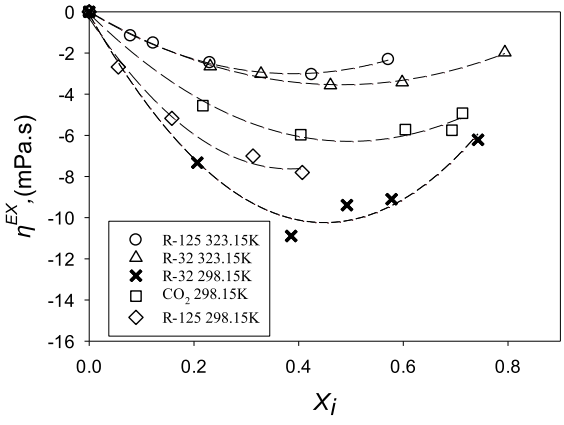

Figure 10. "Excess" viscosity of liquid mixtures of dissolved HFCs and CO_2 in [EMIm][Tf_2N]. Smoothed lines added for visual illustration. (○) R-125 at 323.15 K, (Δ) R-32 at 323.15 K, (X) R-32 at 298.15 K, (□) CO_2 data at 298.15 K from ref 43, and (◊) R-125 at 298.15 K.

https://doi.org/10.1021/acs.iecr.3c03491
Ind. Eng. Chem. Res. 2024, 63, 1151−1169

Table 8. Eyring-NRTL Viscosity Model Adjustable Parameter and Associated % AARD

temperature	Ψ [R-32 (1) + IL (2)]	% AARD	Ψ [R-125 (1) + IL (2)]	% AARD
298.15	16.41	26	5.228	6.6
323.15	16.41	51	5.228	6.7
348.15	16.41	54		

"excess" viscosity at 298.15 K with a magnitude ~2−4X that of the CO_2/[EMIm][Tf_2N] system.[43]

The Eyring-NRTL model[109−113] can be used to predict viscosities of simple liquid mixtures. The fundamental form of the Eyring-NRTL model is

$$\ln(\eta_m \underline{V}_m) = x_1 \ln(\eta_1 \underline{V}_1) + x_2 \ln(\eta_2 \underline{V}_2) - \left.\underline{G}^{EX}\right/_{RT} \quad (22)$$

where $\underline{V}_m$ is the mixture molar volume, $\underline{V}_i$ is the pure component molar volume, and $\underline{G}^{EX}$ is the molar excess Gibbs free energy. The $\underline{G}^{EX}/RT$ term in eq 23 can be evaluated using the NRTL model as follows

$$\left.\underline{G}^{EX}\right/_{RT} = x_1 x_2 \left(\frac{\tau_{21} G_{21}}{x_1 + x_2 G_{21}} + \frac{\tau_{12} G_{12}}{x_2 + x_1 G_{12}} \right) \quad (23)$$

where τ_{ij} and G_{ij} are NRTL model parameters regressed using thermodynamic solubility data as described in Section 3.1. Eqs 23 and 24 are combined and used to predict mixture viscosities for the HFC/IL systems investigated in this study. However, the results obtained using this form of the Eyring-NRTL model resulted in poor predictions (% AARD of up to 35% for R-125/IL). It is worth noting that in Eyring's original work, the Eyring model is divided into two parts—an "ideal" contribution part based on the pure components' viscosities and mole fractions and a "nonideal" contribution part incorporating an excess Gibbs free energy term that may be neglected for systems that behave close to ideality. Furthermore, Eyring weighted the "nonideal" part using an empirical constant (commonly referred to as the "Eyring empirical constant"). Originally, Eyring employed approximately 0.394 as a fixed value for the empirical constant. Here, the Eyring empirical constant is regressed using experimental data to improve the results of the model. The following form of the Eyring-NRTL model can be utilized for the HFC/IL systems of this study

$$\ln(\eta_m \underline{V}_m) = x_1 \ln(\eta_1 \underline{V}_1) + x_2 \ln(\eta_2 \underline{V}_2) - \Psi x_1 x_2 \left(\frac{\tau_{21} G_{21}}{x_1 + x_2 G_{21}} + \frac{\tau_{12} G_{12}}{x_2 + x_1 G_{12}} \right) \quad (24)$$

where Ψ is an adjustable parameter fit to experimental data by minimizing an error objective function (% AARD used here). The adjustable parameters for the systems investigated here and the associated % AARD are reported in Table 8. For the pure HFC viscosity, the saturated liquid-phase viscosity at the specific temperature was used with an added hydrostatic pressure dependency. Pure component HFC liquid viscosities were obtained from REFPROP.[81,114]

The adjusted Eyring-NRTL model successfully predicts the qualitative trends of both systems as illustrated in Figures 11 and 12 but fails to accurately predict the quantitative results for the R-32/[EMIm][Tf_2N] system. It is to be noted that increased parameters of regression may increase the accuracy of the adjusted model; furthermore, increased accuracy at each isotherm can be obtained by regressing the nonideality-

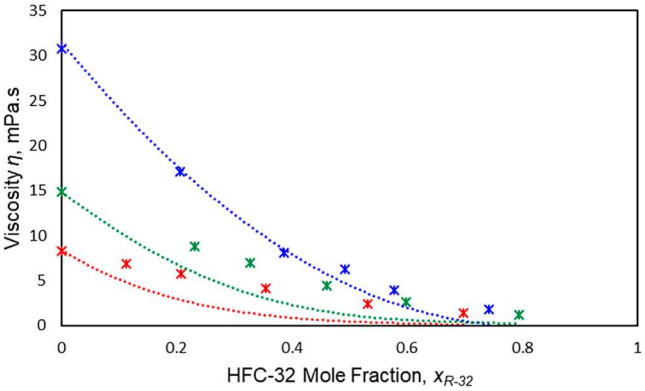

Figure 11. Measured viscosity of R-32/[EMIm][Tf_2N] (blue = 298.15 K; green = 323.15 K; and red = 348.15 K). Lines represent predictions of adjusted Eyring-NRTL model.

weighing parameter at each individual isotherm. Nevertheless, the adjusted model as used here improves the total % AARD by 30% for the R-125/IL system compared to the original, unadjusted Eyring-NRTL model. Predictions using the adjusted model are more accurate for the R-125/[EMIm]-[Tf_2N] system compared to R-32/[EMIm][Tf_2N] as the total % AARD is 6.7% for R-125/IL compared to 44% for the latter R-32/IL system. It is worth noting that for simple liquid systems, the "nonideal" contribution term may be omitted; however, omitting the "nonideal" contribution of the Eyring model results in drastic deviations (>30% AARD) for the R-125/IL system. Yet, the "nonideal" contribution must be adjusted using a scaling factor associated with the excess Gibbs free energy term to properly estimate the "nonideal" contribution.

4.4. Thermal Conductivity. We, as well as other groups, have previously shown that the thermal conductivity of pure IL [EMIm][Tf_2N] decreases with increasing temperature.[74] The thermal conductivity of [EMIm][Tf_2N] saturated with R-125 exhibits a relatively small decrease with increasing dissolved R-125 gas at all three isotherms investigated as shown in Figure 13 and Table 9. The mixtures are in VLE, and higher pressures are used to achieve high compositions of dissolved R-125. At 298.15 K and a R-125 molar composition of 0.63, the percent decrease in thermal conductivity is 6%. At the same molar composition, the percent decrease in thermal conductivity is greater at increased temperatures. The change in thermal conductivity with increasing molar composition of R-125 in the mixture is illustrated in Figure 13; the relative change versus the pure component thermal conductivity is found in Figure S4. In a previous study, the thermal conductivity of an R-134a-saturated [EMIm][Tf_2N] mixture was measured.[74] The thermal conductivity decreases only slightly with increasing molar composition of the gas except at very high compositions of R-134a (>85% mol). In contrast to the large diluent effect of the dissolved gas on the viscosity, the presence of the HFC gases induces very little change in the molecular heat transport mechanism of the pure IL.

https://doi.org/10.1021/acs.iecr.3c03491
Ind. Eng. Chem. Res. 2024, 63, 1151−1169

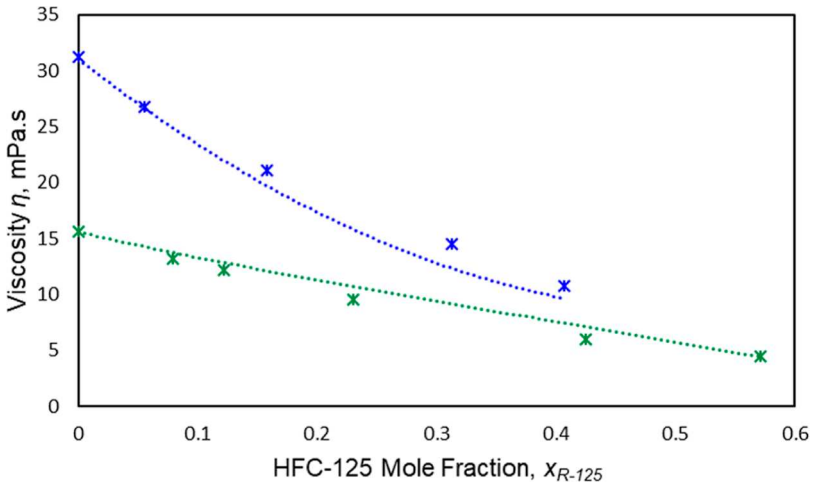

Figure 12. Measured viscosity of R-125/[EMIm][Tf_2N] (blue = 298.15 K and green = 323.15 K). Lines represent predictions of the adjusted Eyring-NRTL model.

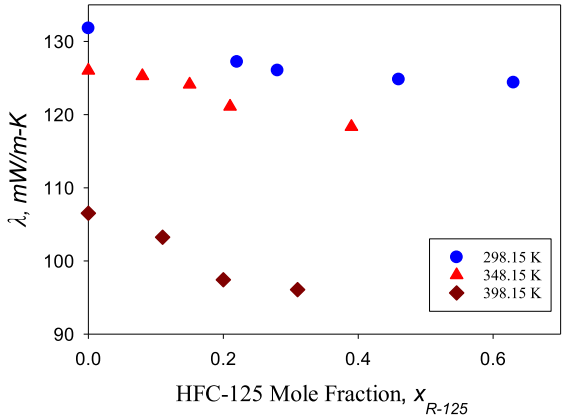

Figure 13. Thermal conductivity of R-125/[EMIm][Tf_2N] at three isotherms and different molar compositions of dissolved R-125. (Blue ●) 298.15 K, (red ■) 348.15 K, and (brown ♦) 398.15 K.

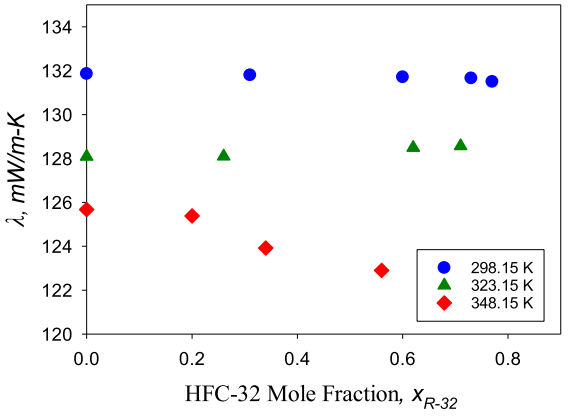

Figure 14. Thermal conductivity of R-32/[EMIm][Tf_2N] at three isotherms and different molar compositions of dissolved R-32. (Blue ●) 298.15 K, (green ▲) 348.15 K, and (red ♦) 348.15 K.

The thermal conductivity of the R-32/[EMIm][Tf_2N] system is reported in Table 9 and illustrated in Figure 14. Interestingly, the R-32 system behaves much differently than either of the R-125/[EMIm][Tf_2N] system or the R-134a/

Table 9. Thermal Conductivity of R-125/[EMIm][Tf_2N] and R-32/[EMIm][Tf_2N][a]

R-125/[EMIm][Tf_2N]			R-32/[EMIm][Tf_2N]		
T [K]	x_{R-125}	λ [mW/m K]	T [K]	x_{R-32}	λ [mW/m K]
298.15[b]	0.00[b]	131.82	298.15[b]	0.00[d]	131.86
	0.22	127.23		0.31	131.8
	0.28	126.06		0.60	131.71
	0.46	124.82		0.73	131.5
	0.63	124.40		0.77	131.66
348.15[b]	0.00[d]	126.03	323.15[b]	0.00[d]	124.09
	0.08	125.28		0.26	124.1
	0.15	124.13		0.62	124.49
	0.21	121.11		0.71	124.57
	0.39	118.34			
398.15[c]	0.00	106.52	348.15[b]	0.00[d]	125.67
	0.11	103.23		0.20	125.38
	0.20	97.43		0.34	123.92
	0.31	96.07		0.56	122.9

[a]Reported standard uncertainties: $u(T)$ = 0.1 K, $u(\lambda)$ = 2.5 mW/m·K (reported as highest uncertainty of all measurements), and $u(x)$ = 0.05 (reported as highest uncertainty of all data points). [b]Compositions interpolated/extrapolated from measured VLE data. [c]Compositions predicted using EoS. [d]Pure IL at ambient pressure (gauge).

https://doi.org/10.1021/acs.iecr.3c03491
Ind. Eng. Chem. Res. 2024, 63, 1151−1169

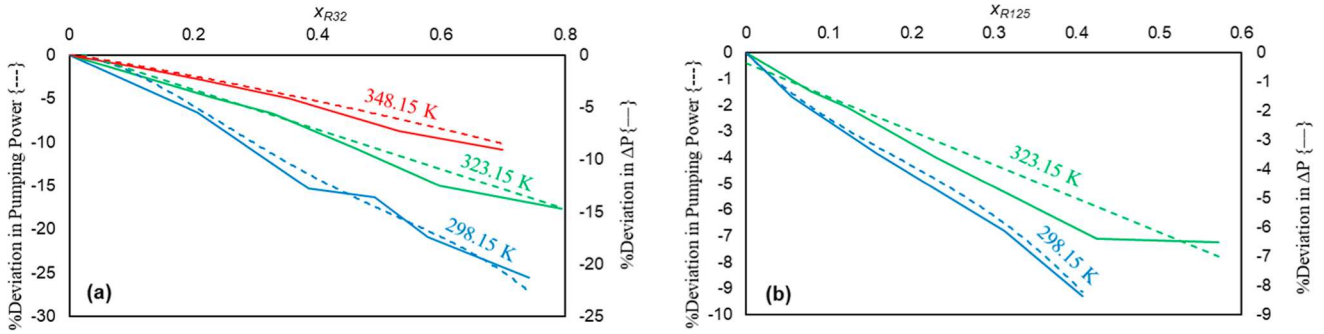

Figure 15. (a) Deviation in pumping power (dashed lines—left axis) for a system utilizing R-32/[EMIm][Tf_2N] with mixture viscosities calculated using a mole-average mixing rule relative to a system utilizing measured mixture viscosities and (b) for R-125/[EMIm][Tf_2N]. Solid lines represent deviations in pressure drop (right axis).

[EMIm][Tf_2N] system.[74] The change in thermal conductivity is much less pronounced. At 298.15 and 323.15 K, the thermal conductivity is nearly constant throughout the investigated composition regimes (within experimental uncertainty); relative change versus the pure component thermal conductivity is found in Figure S5. The apparent subtle change in thermal conductivity is less than the uncertainty range associated with the methodology employed in this study. Hence, it is inconclusive whether there might truly exist an, albeit small, increase, decrease, or a minimum at the two initial isotherms. However, at the 348.15 K isotherm, a more pronounced decrease is observed with a percent decrease of 2.4% achieved at a dissolved R-32 molar composition of 0.56. It is worth noting that the saturated liquid thermal conductivity of R-32 at 298.15 K is 125.89 mW/m K with a subcooled liquid thermal conductivity to pressure sensitivity, $\partial\lambda/\partial P$, of 0.13 mW/m bar K.[81,114] Similarly, the saturated liquid thermal conductivity at 323.15 K is 107.03 mW/m K. In contrast, the thermal conductivity of saturated liquid R-134a at 298.15 K is 81.134 mW/m K and that of R-125 is 59.422 mW/m K.[81,114,115] The unusually high thermal conductivity of liquid R-32 compared to that of other HFCs may play a role in the differing behavior in thermal conductivity of the HFC/IL mixtures containing R-32. R-32 has higher vapor pressure than either of the aforementioned HFCs and a thermal conductivity of closer proximity to that of the pure IL. Hence, the combination of these two characteristics may lead to the observed behavior of nearly constant thermal conductivity even at moderate compositions of dissolved R-32 in the IL.

In our previous study, we have shown that the thermal conductivity of CO_2-saturated [HMIm][Tf_2N] increases in certain regions of solubility.[10] This phenomenon appears to be due to the increased pressures required to dissolve CO_2 in the IL to a certain composition. Hence, the hydrostatic pressure exerted may cause an increase in mixture thermal conductivity and we have shown for the pure IL thermal conductivity. However, since the pressures required to dissolve R-134a and R-125 in the investigated ILs are much lower than those needed for CO_2 dissolution, hydrostatic pressure effects do not have observable contributions that may outweigh the slight diluent effects. In contrast, R-32 has similar thermal conductivity to that of the IL; hence, large diluent effects are not expected. Yet, R-32 dissolves at much lower pressure regimes than CO_2. Therefore, the R-32/IL system is expected to exhibit only a slight diluent effect and a relatively slight hydrostatic pressure effect with regard to changes in thermal conductivity.

4.5. Engineering Ramifications. The data presented in this study demonstrate that transport properties often may not be accurately predicted with simple commonly employed mixing rules. Mixing rules based on compositional averages (mole fraction, mass fraction, volume fraction, etc.) of the pure components' properties at the same temperature (and pressure) may lead to erroneous approximations. Such mispredictions may propagate to drastic errors in the understanding of heat, mass, or momentum transfer, sizing of engineering unit operations, etc. Two common examples in engineering applications are pumping power needed for pipe transport and a simple heat exchanger in processes involving HFC/IL mixtures.[116−119] The heat exchanger could be used to heat or cool the mixture, or potentially as a reboiler in an extractive distillation unit.

4.5.1. Pumping Power and Viscosity. To assess the potential effects of approximated mixture viscosity values using composition average mixing rules (versus measured), a hypothetical calculation using the Fanning equation for pressure drop in a system utilizing the HFC/IL mixtures investigated in this study is carried out as presented in detail in the Supporting Information. Figure 15a,b illustrates the underprediction of both pressure drop and pumping power that may result through the use of simple composition-based linear mixing rules to predict the viscosity of HFC/IL mixtures relative to assessments made using measured mixture viscosity data.

The effects of using simple mixing rules to predict pumping power and pressure drop are more pronounced in the R-32/IL mixture than the R-125/IL mixture. This can be attributed to the larger difference between the viscosities of the pure components in the former system. The absolute excess viscosity of the R-125/IL system is less than that of the R-32/IL system at 298.15 and 323.15 K as illustrated in Figure 10. In fact, the deviation difference in the pressure drop can be correlated with the magnitude of excess viscosity. To a similar effect, the deviation in pumping power and pressure drop decreases with increasing temperature. The pure IL viscosity exhibits larger decreases with temperature than the pure component HFCs—$\partial\eta/\partial T$ values for R-32, R-125, and [EMIm][Tf_2N] are −0.0013, −0.0021, and −0.56 mPa s/K, respectively. The viscosities of the pure components exhibit decreasing differences with increasing temperature (*the excess viscosity decreases with increasing temperature*), and thus, the deviations in pumping duty and pressure drop decrease.

4.5.2. Heat Exchanger Design: Combined Effects of Density, Viscosity, and Thermal Conductivity. The area of

https://doi.org/10.1021/acs.iecr.3c03491
Ind. Eng. Chem. Res. 2024, 63, 1151−1169

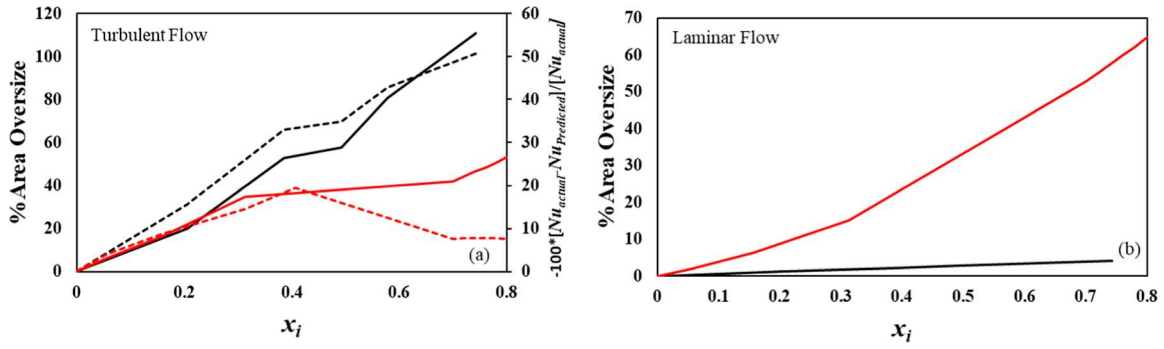

Figure 16. % Area oversize (left axis) of a heat exchanger and Nusselt number deviations (right axis) due to weighted-average mixing rule predictions for thermal conductivity, viscosity, and density in a shell and tube heat exchanger operating in the fully developed turbulent flow regime (a) and laminar flow regime with constant surface heat flux (b). Red lines are R-125/IL. Black lines are R-32/IL. Dashed lines are negative deviations in Nusselt number. At 298.15 K.

heat exchange required to achieve desired heating/cooling duty is implicit in viscosity, density, and thermal conductivity. A procedure to estimate the required area of heat exchange and relevant equations are presented in the Supporting Information. The employed procedure utilizes the Nusselt number correlation, which defines the ratio of convective heat transfer to conductive heat transfer with functionalities of viscous flow, density, and thermal conductivity. The thermal conductivity for most HFC/IL systems cannot be accurately approximated using simple mole fraction-averaged mixing rules. The same argument is made for the viscosity of the mixtures. Typical mixing rules for liquid systems found in the literature struggle in accurately capturing the behavior of the two aforementioned properties. In contrast, rigorous equations of state with appropriate mixing rules may often lead to acceptable approximations of the mixture densities.

Heat exchanger design often employs turbulent flow configurations as turbulent flow regimes are typically associated with increased heat transfer and thus reduced area of heat exchange.[120] Figure 16a illustrates the percent overprediction of the area of heat exchange resulting from the use of a simple weighted-average linear mixing rule of the pure component thermal conductivities, viscosities, and densities in a heat exchanger operating in the fully developed turbulent flow regime with a constant flow velocity and hydraulic diameter. Figure 16b illustrates the percent overprediction in the laminar flow regime with a constant surface heat flux. The applied mixing rules use a mole fraction linear average for viscosity and thermal conductivity and a mass fraction average for the mass density.

As demonstrated in Figure 16, mixing rules based on pure component properties can result in large unit design ramifications. In the laminar regime (Figure 16b), the required area of heat exchange can be overpredicted by ∼65% at an R-125 mol composition of ∼80% in [EMIm][Tf_2N] due to the significant differences between the thermal conductivities of the pure components. It is common engineering practice to oversize the surface area than the exact specification due to anticipated changes in performance, e.g., fouling and changes in the process. However, the addition to the already overpredicted surface area would lead to further expenditure than is needed. The R-32/IL system exhibits less pronounced overpredictions in the laminar flow regime as the evaluation of the required area of heat exchange in the laminar regime does not include a viscosity and density functionality. Additionally, the thermal conductivity of saturated liquid R-32 at 298.15 K is similar to that of the IL; hence, a weighted-average mixing rule would result in less absolute deviation. Very few HFC components would have a similar thermal conductivity to the IL, so the results with R-125 would be more typical.

In the turbulent flow regime, the R-32/IL system exhibits higher deviations at moderate-to-high solute compositions as a result of the elevated excess viscosity exhibited by the R-32/IL system and the larger differences between the pure component mass densities relative to the R-125/IL system. In fact, at a respective dissolved solute composition of 50%, the R-32/IL system exhibits an overprediction of 58% compared to 40% in the R-125/IL system. Costs generally scale with surface area; thus, capital costs would be overpredicted.

5. CONCLUSIONS

VLE data (solubility) of HFC gases pentafluoroethane (R-125) and difluoromethane (R-32) in the IL, [EMIm][Tf_2N], have been measured to 4 MPa and temperatures up to 398.15 K. The solubility of R-32 in the IL is higher than that of R-125 at the same temperature and pressure. Pressures and compositions of dissolved R-32 are extended to establish the lower critical and UCEPs of the mixture demonstrating that R-32 exhibits a vapor−liquid−liquid line spanning a temperature regime of ∼14 K compared to 69.17 K for the R-125/[EMIm][Tf_2N] system (LCEP to UCEP). The solubility data can be successfully correlated using the NRTL model and Peng−Robinson EoS coupled with the Boston−Mathias−van der Waals-2 mixing rule. The NRTL model captures the vapor−liquid−liquid regions for the R-125/IL system but fails to capture that of the R-32/IL system. The Peng−Robinson EoS successfully captures experimentally confirmed VLLE regions for R-125/IL at 298.15 and 323.15 K and at 348.15 K for the R-32/IL system.

The density, viscosity, and thermal conductivity of the mixtures exhibit considerably varying behavior with increasing composition of the dissolved HFC in the liquid phase. The density of the R-125/IL system remains relatively constant (1%) with increasing molar composition of dissolved HFC while that of R-32 exhibits a relatively larger decrease (4−6%) at low-to-moderate dissolved HFC compositions. The excess molar volume of both systems is negative with magnitudes exceeding those exhibited by typical organic liquid mixtures signifying increased attractive interactions.

The viscosity of both systems exhibits drastic decreases with increasing HFC composition. The decrease in the R-32 system is larger than that of the R-125 system at all temperatures

https://doi.org/10.1021/acs.iecr.3c03491
Ind. Eng. Chem. Res. 2024, 63, 1151−1169

investigated. The excess viscosity is negative for both mixtures at the conditions probed with those of R-32/IL being larger in magnitude than those of R-125/IL due to the lower pure component viscosity and higher dielectric constant of R-32 compared to R-125. The excess viscosity decreases in magnitude with increasing temperature as the change in viscosity with temperature for the pure IL is greater than those of the pure HFCs.

The thermal conductivity of the R-125/IL system is investigated at temperatures up to 398.15 K and compositions to 65% mol_{HFC}. The thermal conductivity of the mixture remains similar to that of the pure IL with increasing change in thermal conductivity at higher temperatures. R-32 has a pure component thermal conductivity similar to that of the IL at lower temperatures, and a change in thermal conductivity from that of the pure component IL is not observed except at higher temperatures where the difference between the pure component thermal conductivities is more pronounced. Nevertheless, at all compositions investigated for both systems (<80% mol_{HFC}), the IL retains its thermal conduction abilities, indicating that the relatively low solvation potential of the HFCs inhibits them from drastically altering the structure of the IL at the conditions investigated.

The thermodynamic/transport properties investigated demonstrate highly nonideal systems. Using linear weighted-average mixing rules to design unit operations involving the mixtures probed here results in highly erroneous approximations of the transport/thermodynamic properties. Such approximations can result in underpredictions of pumping power to more than 25% and overpredictions in the area of heat exchange required by more than 100%. Thus, a better understanding of molecular behavior and rigorous thermophysical models is needed for more reliable predictive techniques of mixture transport properties.

■ ASSOCIATED CONTENT

Supporting Information

The Supporting Information is available free of charge at https://pubs.acs.org/doi/10.1021/acs.iecr.3c03491.

Solubility data in various units and volume expansions; simplified schematic of the measuring apparatus for viscosity, density, and solubility; sensitivity analysis of the NRTL model parameters; percent decrease in viscosity with molar composition; change in thermal conductivity with molar composition; and detailed methodology for assessing the ramifications on unit design (PDF)

■ AUTHOR INFORMATION

Corresponding Author

Aaron M. Scurto − *Department of Chemical & Petroleum Engineering, University of Kansas, Lawrence, Kansas 66045, United States; Institute for Sustainable Engineering, University of Kansas, Lawrence, Kansas 66045, United States;* orcid.org/0000-0001-7214-1871; Phone: (785) 864-4947; Email: ascurto@ku.edu; Fax: (785) 864-4967

Authors

Karim S. Al-Barghouti − *Department of Chemical & Petroleum Engineering, University of Kansas, Lawrence, Kansas 66045, United States; Institute for Sustainable Engineering, University of Kansas, Lawrence, Kansas 66045, United States;* orcid.org/0000-0002-6167-1516

Kalin R. Baca − *Department of Chemical & Petroleum Engineering, University of Kansas, Lawrence, Kansas 66045, United States; Institute for Sustainable Engineering, University of Kansas, Lawrence, Kansas 66045, United States;* orcid.org/0000-0002-7292-8698

Mark B. Shiflett − *Department of Chemical & Petroleum Engineering, University of Kansas, Lawrence, Kansas 66045, United States; Institute for Sustainable Engineering, University of Kansas, Lawrence, Kansas 66045, United States;* orcid.org/0000-0002-8934-6192

Complete contact information is available at: https://pubs.acs.org/10.1021/acs.iecr.3c03491

Notes

The authors declare no competing financial interest.

■ ACKNOWLEDGMENTS

We would like to thank the US National Science Foundations (NSF) for financial support under grants EEC-1852308 and EFRI-2029354. We would also like to thank Dr. Luke Simoni at the Chemours Company for generous donation of the HFC gases.

■ REFERENCES

(1) Kim, Y. J.; Gonzalez, M. Exergy analysis of an ionic-liquid absorption refrigeration system utilizing waste-heat from datacenters. *Int. J. Refrig.* **2014**, *48*, 26−37.

(2) Kim, Y. J.; Kim, S.; Joshi, Y. K.; Fedorov, A. G.; Kohl, P. A. Thermodynamic analysis of an absorption refrigeration system with ionic-liquid/refrigerant mixture as a working fluid. *Energy* **2012**, *44* (1), 1005−1016.

(3) Moreno, D.; Ferro, V. R.; De Riva, J.; Santiago, R.; Moya, C.; Larriba, M.; Palomar, J. Absorption refrigeration cycles based on ionic liquids: Refrigerant/absorbent selection by thermodynamic and process analysis. *Appl. Energy* **2018**, *213*, 179−194.

(4) Sen, M.; Paolucci, S. Using Carbon Dioxide and Ionic Liquids for Absorption Refrigeration. *7th IIR Gustav Lorentzen Conference on Natural Working Fluids*; IIF-IIR: Trondheim, Norway, 2006.

(5) Mark Brandon Shiflett, A. Y. Absorption Cycle Utilizing Ionic Liquid as Working Fluid. WO2006084262A1, 2006.

(6) Aghaie, M.; Rezaei, N.; Zendehboudi, S. A systematic review on CO_2 capture with ionic liquids: Current status and future prospects. *Renewable Sustainable Energy Rev.* **2018**, *96*, 502−525.

(7) Brennecke, J. F.; Gurkan, B. E. Ionic Liquids for CO_2 Capture and Emission Reduction. *J. Phys. Chem. Lett.* **2010**, *1* (24), 3459−3464.

(8) Ramdin, M.; De Loos, T. W.; Vlugt, T. J. H. State-of-the-Art of CO_2 Capture with Ionic Liquids. *Ind. Eng. Chem. Res.* **2012**, *51* (24), 8149−8177.

(9) Shiflett, M. B.; Drew, D. W.; Cantini, R. A.; Yokozeki, A. Carbon Dioxide Capture Using Ionic Liquid 1-Butyl-3-methylimidazolium Acetate. *Energy Fuels* **2010**, *24* (10), 5781−5789.

(10) Al-Barghouti, K. S.; Scurto, A. M. Thermal conductivity of the ionic liquid [HMIm] [Tf_2N] with compressed carbon dioxide. *AIChE J.* **2022**, *68* (6), No. e17635.

(11) Kermani, N. A. Design and prototyping of an ionic liquid piston compressor as a new generation of compressors for hydrogen refueling stations. Ph.D. Thesis, Technical University of Denmark, Kgs, Lyngby, 2017.

(12) Predel, T.; Schlücker, E. Ionic Liquids in Oxygen Compression. *Chem. Eng. Technol.* **2009**, *32* (8), 1183−1188.

(13) Afzal, W.; Liu, X.; Prausnitz, J. M. Physical data for a process to separate krypton from air by selective absorption in an ionic liquid. *Fluid Phase Equilib.* **2015**, *404*, 124−130.

(14) Morais, A. R. C.; Harders, A. N.; Baca, K. R.; Olsen, G. M.; Befort, B. J.; Dowling, A. W.; Maginn, E. J.; Shiflett, M. B. Phase Equilibria, Diffusivities, and Equation of State Modeling of HFC-32 and HFC-125 in Imidazolium-Based Ionic Liquids for the Separation of R-410A. *Ind. Eng. Chem. Res.* **2020**, *59* (40), 18222−18235.
(15) Shiflett, M. B.; Yokozeki, A. Utilizing ionic liquids for hydrofluorocarbon separation. U.S. Patent 8,628,644 B2, 2006.
(16) Asensio-Delgado, S.; Pardo, F.; Zarca, G.; Urtiaga, A. Enhanced absorption separation of hydrofluorocarbon/hydrofluoroolefin refrigerant blends using ionic liquids. *Sep. Purif. Technol.* **2020**, *249*, 117136.
(17) Asensio-Delgado, S.; Pardo, F.; Zarca, G.; Urtiaga, A. Absorption separation of fluorinated refrigerant gases with ionic liquids: Equilibrium, mass transport, and process design. *Sep. Purif. Technol.* **2021**, *276*, 119363.
(18) Booten, C.; Nicholson, S.; Mann, M.; Abdelaziz, O. *Refrigerants: Market Trends and Supply Chain Assessment*; Office of Scientific and Technical Information (OSTI), 2020.
(19) ASHRAE. Designation and Safety Classification of Refrigerants. *ANSI/ASHRAE Standard 34−2019 Designation and Safety Classification of Refrigerants; American Society of Heating, Refrigerating and Air-Conditioning Engineers*; ANSI, 2019.
(20) Ebnesajjad, S. *Concise Handbook of Fluorocarbon Gases: Applications in Refrigeration and Other Industries*; John Wiley & Sons, 2021.
(21) EPA. *Recent International Developments under the Montreal Protocol*. 2016. https://www.epa.gov/ozone-layer-protection/recent-international-developments-under-montreal-protocol (accessed 2021).
(22) EPA. *Protecting Our Climate by Reducing Use of HFCs*. 2021. https://www.epa.gov/climate-hfcs-reduction (accessed 2021).
(23) EEA. *Hydrofluorocarbon phase-down in Europe*. 2021. https://www.eea.europa.eu/ims/hydrofluorocarbon-phase-down-in-europe (accessed 2021).
(24) Harders, A. N.; Sturd, E. R.; Vallier, J. E.; Corbin, D. R.; White, W. R.; Junk, C. P.; Shiflett, M. B. Selective separation of HFC-32 from R-410A using poly(dimethylsiloxane) and a copolymer of perfluoro-(butenyl vinyl ether) and perfluoro (2,2-dimethyl-1,3-dioxole). *J. Membr. Sci.* **2022**, *652*, 120467.
(25) Yancey, A. D.; Corbin, D. R.; Shiflett, M. B. Difluoromethane (HFC-32) and Pentafluoroethane (HFC-125) Sorption on Linde Type A (LTA) Zeolites for the Separation of Azeotropic Hydrofluorocarbon Refrigerant Mixtures. *Langmuir* **2022**, *38* (6), 1937−1953.
(26) Sosa, J. E.; Malheiro, C.; Ribeiro, R. P.; Castro, P. J.; Piñeiro, M. M.; Araújo, J. M.; Plantier, F.; Mota, J. P.; Pereiro, A. B. Adsorption of fluorinated greenhouse gases on activated carbons: evaluation of their potential for gas separation. *J. Chem. Technol. Biotechnol.* **2020**, *95*, 1892−1905.
(27) Pardo, F.; Zarca, G.; Urtiaga, A. Effect of feed pressure and long-term separation performance of Pebax-ionic liquid membranes for the recovery of difluoromethane (R32) from refrigerant mixture R410A. *J. Membr. Sci.* **2021**, *618*, 118744.
(28) Yancey, A. D.; Terian, S. J.; Shaw, B. J.; Bish, T. M.; Corbin, D. R.; Shiflett, M. B. A review of fluorocarbon sorption on porous materials. *Microporous Mesoporous Mater.* **2022**, *331*, 111654.
(29) Baca, K. R.; Olsen, G. M.; Matamoros Valenciano, L.; Bennett, M. G.; Haggard, D. M.; Befort, B. J.; Garciadiego, A.; Dowling, A. W.; Maginn, E. J.; Shiflett, M. B. Phase Equilibria and Diffusivities of HFC-32 and HFC-125 in Ionic Liquids for the Separation of R-410A. *ACS Sustain. Chem. Eng.* **2022**, *10* (2), 816−830.
(30) Finberg, E. A.; Shiflett, M. B. Process Designs for Separating R-410A, R-404A, and R-407C Using Extractive Distillation and Ionic Liquid Entrainers. *Ind. Eng. Chem. Res.* **2021**, *60* (44), 16054−16067.
(31) Asensio-Delgado, S.; Jovell, D.; Zarca, G.; Urtiaga, A.; Llovell, F. Thermodynamic and process modeling of the recovery of R410A compounds with ionic liquids. *Int. J. Refrig.* **2020**, *118*, 365−375.
(32) Shiflett, M. B.; Harmer, M. A.; Junk, C. P.; Yokozeki, A. Solubility and diffusivity of 1,1,1,2-tetrafluoroethane in room-temperature ionic liquids. *Fluid Phase Equilib.* **2006**, *242* (2), 220−232.
(33) Shiflett, M. B.; Yokozeki, A. Solubility and diffusivity of hydrofluorocarbons in room-temperature ionic liquids. *AIChE J.* **2006**, *52* (3), 1205−1219.
(34) Esaki, T.; Kobayashi, N.; Uchiyama, H.; Matsukuma, Y. Characteristics of Absorption Equilibrium with HFC-134a and an Ionic Liquid Pair. *J. Mater. Sci. Chem. Eng.* **2019**, *07* (03), 65−78.
(35) Liu, X.; Pan, P.; He, M. Vapor-liquid equilibrium and diffusion coefficients of R32+[HMIM] [FEP], R152a+[HMIM] [FEP] and R161+[HMIM] [FEP]. *J. Mol. Liq.* **2018**, *253*, 28−35.
(36) Ren, W.; Scurto, A. M. Phase equilibria of imidazolium ionic liquids and the refrigerant gas, 1,1,1,2-tetrafluoroethane (R-134a). *Fluid Phase Equilib.* **2009**, *286* (1), 1−7.
(37) Ren, W.; Scurto, A. M.; Shiflett, M. B.; Yokozeki, A. Phase Behavior and Equilibria of Ionic Liquids and Refrigerants: 1-Ethyl-3-methyl-imidazolium Bis(trifluoromethylsulfonyl)imide ([EMIm]-[Tf2N]) and R-134a. In *Gas-Expanded Liquids and Near-Critical Media*; Hutchenson, K. W., Scurto, A. M., Subramaniam, B., Eds.; American Chemical Society, 2009; Vol. *1006*, pp 112−128.
(38) Sosa, J. E.; Ribeiro, R. P. P. L.; Castro, P. J.; Mota, J. P. B.; Araújo, J. M. M.; Pereiro, A. B. Absorption of Fluorinated Greenhouse Gases Using Fluorinated Ionic Liquids. *Ind. Eng. Chem. Res.* **2019**, *58* (45), 20769−20778.
(39) Sousa, J. M. M. V.; Granjo, J. F. O.; Queimada, A. J.; Ferreira, A. G. M.; Oliveira, N. M. C.; Fonseca, I. M. A. Solubilities of hydrofluorocarbons in ionic liquids: Experimental and modelling study. *J. Chem. Thermodyn.* **2014**, *73*, 36−43.
(40) Shiflett, M. B.; Harmer, M. A.; Junk, C. P.; Yokozeki, A. Solubility and Diffusivity of Difluoromethane in Room-Temperature Ionic Liquids. *J. Chem. Eng. Data* **2006**, *51* (2), 483−495.
(41) Shiflett, M. B.; Yokozeki, A. Binary Vapor-Liquid and Vapor-Liquid-Liquid Equilibria of Hydrofluorocarbons (HFC-125 and HFC-143a) and Hydrofluoroethers (HFE-125 and HFE-143a) with Ionic Liquid [emim] [Tf_2N]. *J. Chem. Eng. Data* **2008**, *53* (2), 492−497.
(42) Finberg, E. Refrigerant Separation with Extractive Distillation Using Ionic Liquid Entrainers. M.S. Thesis, University of Kansas, 2022.
(43) Ahosseini, A.; Ortega, E.; Sensenich, B.; Scurto, A. M. Viscosity of n-alkyl-3-methyl-imidazolium bis(trifluoromethylsulfonyl)amide ionic liquids saturated with compressed CO_2. *Fluid Phase Equilib.* **2009**, *286* (1), 72−78.
(44) Morais, A. R. C.; Alaras, L. M.; Baek, D. L.; Fox, R. V.; Shiflett, M. B.; Scurto, A. M. Viscosity of 1-Alkyl-1-methylpyrrolidinium Bis(trifluoromethylsulfonyl)imide Ionic Liquids Saturated with Compressed CO_2. *J. Chem. Eng. Data* **2019**, *64* (11), 4658−4667.
(45) Ren, W.; Ahosseini, A.; Scurto, A. M. I&EC 16-Phase equilibria, viscosity, and diffusivity of imidazolium ionic liquids with compressed carbon dioxide and hydrofluorocarbon gases. *Abstr. Pap. Am. Chem. Soc.* **2008**, *236*.
(46) Tomida, D.; Kenmochi, S.; Qiao, K.; Bao, Q.; Yokoyama, C. Viscosity of ionic liquid mixtures of 1-alkyl-3-methylimidazolium hexafluorophosphate+CO_2. *Fluid Phase Equilib.* **2011**, *307* (2), 185−189.
(47) Tomida, D.; Kumagai, A.; Qiao, K.; Yokoyama, C. Viscosity of 1-Butyl-3-methylimidazolium Hexafluorophosphate + CO_2 Mixture. *J. Chem. Eng. Data* **2007**, *52* (5), 1638−1640.
(48) Dyson, P. J.; Laurenczy, G. Determination of the Viscosity of the Ionic Liquids [bmim] [PF_6] and [bmim] [TF_2N] Under High CO_2 Gas Pressure Using Sapphire NMR Tubes. *Z. Naturforsch., B: J. Chem. Sci.* **2008**, *63* (6), 681−684.
(49) Liu, Z.; Wu, W.; Han, B.; Dong, Z.; Zhao, G.; Wang, J.; Jiang, T.; Yang, G. Study on the Phase Behaviors, Viscosities, and Thermodynamic Properties of CO_2/[C4mim] [PF_6]/Methanol System at Elevated Pressures. *Chem.—Eur. J.* **2003**, *9* (16), 3897−3903.
(50) Ahosseini, A.; Ren, W.; Weatherley, L. R.; Scurto, A. M. Viscosity and self-diffusivity of ionic liquids with compressed hydrofluorocarbons: 1-Hexyl-3-methyl-imidazolium bis-

https://doi.org/10.1021/acs.iecr.3c03491
Ind. Eng. Chem. Res. 2024, 63, 1151−1169

(trifluoromethylsulfonyl)amide and 1,1,1,2-tetrafluoroethane. *Fluid Phase Equilib.* **2017**, *437*, 34−42.
(51) Wang, N.; Zhang, Y.; Al-Barghouti, K. S.; Kore, R.; Scurto, A. M.; Maginn, E. J. Structure and Dynamics of Hydrofluorocarbon/Ionic Liquid Mixtures: An Experimental and Molecular Dynamics Study. *J. Phys. Chem. B* **2022**, *126* (41), 8309−8321.
(52) Yokozeki, A.; Shiflett, M. B. Global phase behaviors of trifluoromethane in ionic liquid [bmim] [PF_6]. *AIChE J.* **2006**, *52* (11), 3952−3957.
(53) Shiflett, M. B.; Yokozeki, A. Solubility Differences of Halocarbon Isomers in Ionic Liquid [emim] [Tf2N]. *J. Chem. Eng. Data* **2007**, *52* (5), 2007−2015.
(54) Shiflett, M. B.; Yokozeki, A. Vapor-Liquid-Liquid Equilibria of Hydrofluorocarbons + 1-Butyl-3-methylimidazolium Hexafluorophosphate. *J. Chem. Eng. Data* **2006**, *51* (5), 1931−1939.
(55) Shiflett, M. B.; Yokozeki, A. Vapor-Liquid-Liquid Equilibria of Pentafluoroethane and Ionic Liquid [bmim] [PF_6] Mixtures Studied with the Volumetric Method. *J. Phys. Chem. B* **2006**, *110* (29), 14436−14443.
(56) Zhang, Y.; Jia, X.; Wang, X. Experimental investigation on the viscosity of [Hmim] [Tf2N] saturated with R1234ze(E) or R1234yf. *Int. J. Refrig.* **2020**, *117*, 338−345.
(57) Gardas, R. L.; Coutinho, J. A. P. Group contribution methods for the prediction of thermophysical and transport properties of ionic liquids. *AIChE J.* **2009**, *55* (5), 1274−1290.
(58) Gardas, R. L.; Ge, R.; Goodrich, P.; Hardacre, C.; Hussain, A.; Rooney, D. W. Thermophysical Properties of Amino Acid-Based Ionic Liquids. *J. Chem. Eng. Data* **2010**, *55* (4), 1505−1515.
(59) Hezave, A. Z.; Raeissi, S.; Lashkarbolooki, M. Estimation of Thermal Conductivity of Ionic Liquids Using a Perceptron Neural Network. *Ind. Eng. Chem. Res.* **2012**, *51* (29), 9886−9893.
(60) Koller, T. M.; Schmid, S. R.; Sachnov, S. J.; Rausch, M. H.; Wasserscheid, P.; Fröba, A. P. Measurement and Prediction of the Thermal Conductivity of Tricyanomethanide- and Tetracyanoborate-Based Imidazolium Ionic Liquids. *Int. J. Thermophys.* **2014**, *35* (2), 195−217.
(61) Nieto De Castro, C. A.; Lourenço, M. J. V.; Ribeiro, A. P. C.; Langa, E.; Vieira, S. I. C.; Goodrich, P.; Hardacre, C. Thermal Properties of Ionic Liquids and IoNanofluids of Imidazolium and Pyrrolidinium Liquids. *J. Chem. Eng. Data* **2010**, *55* (2), 653−661.
(62) Oster, K.; Goodrich, P.; Jacquemin, J.; Hardacre, C.; Ribeiro, A. P. C.; Elsinawi, A. A new insight into pure and water-saturated quaternary phosphonium-based carboxylate ionic liquids: Density, heat capacity, ionic conductivity, thermogravimetric analysis, thermal conductivity and viscosity. *J. Chem. Thermodyn.* **2018**, *121*, 97−111.
(63) Rodil, E.; Arce, A.; Arce, A.; Soto, A. Measurements of the density, refractive index, electrical conductivity, thermal conductivity and dynamic viscosity for tributylmethylphosphonium and methylsulfate based ionic liquids. *Thermochim. Acta* **2018**, *664*, 81−90.
(64) Valkenburg, M. E. V.; Vaughn, R. L.; Williams, M.; Wilkes, J. S. Thermochemistry of ionic liquid heat-transfer fluids. *Thermochim. Acta* **2005**, *425* (1−2), 181−188.
(65) Wu, K.-J.; Zhao, C.-X.; He, C.-H. Development of a group contribution method for determination of thermal conductivity of ionic liquids. *Fluid Phase Equilib.* **2013**, *339*, 10−14.
(66) Zaripov, Z. I.; Gumerov, F. M.; Khairutdinov, V. F.; Małgorzata, M.; Edward, Z.; Marzena, D.; Abdulagatov, I. M. Thermal conductivity and thermal diffusivity of Pyrrolidinium-BasedIonic liquids at atmospheric pressure. *Fluid Phase Equilib.* **2019**, *485*, 135−145.
(67) Chen, Q. L.; Wu, K. J.; He, C. H. Thermal Conductivity of Ionic Liquids at Atmospheric Pressure: Database, Analysis, and Prediction Using a Topological Index Method. *Ind. Eng. Chem. Res.* **2014**, *53* (17), 7224−7232.
(68) Wu, K.-J.; Chen, Q.-L.; He, C.-H. Speed of sound of ionic liquids: Database, estimation, and its application for thermal conductivity prediction. *AIChE J.* **2014**, *60* (3), 1120−1131.
(69) Yebra, F.; Troncoso, J.; Romaní, L. Thermal conductivity of ionic liquids under pressure. *Fluid Phase Equilib.* **2020**, *515*, 112573.
(70) Tomida, D.; Kenmochi, S.; Tsukada, T.; Qiao, K.; Yokoyama, C. Thermal Conductivities of [bmim] [PF_6], [hmim] [PF_6], and [omim] [PF_6] from 294 to 335 K at Pressures up to 20 MPa. *Int. J. Thermophys.* **2007**, *28* (4), 1147−1160.
(71) Rausch, M. H.; Heller, A.; Herbst, J.; Koller, T. M.; Bahlmann, M.; Schulz, P. S.; Wasserscheid, P.; Fröba, A. P. Mutual and Thermal Diffusivity of Binary Mixtures of the Ionic Liquids [BMIM] [$C(CN)_3$] and [BMIM] [$B(CN)_4$] with Dissolved CO_2 by Dynamic Light Scattering. *J. Phys. Chem. B* **2014**, *118* (17), 4636−4646.
(72) Klein, T.; Piszko, M.; Lang, M.; Mehler, J.; Schulz, P. S.; Rausch, M. H.; Giraudet, C.; Koller, T. M.; Fröba, A. P. Diffusivities in Binary Mixtures of [AMIM] [NTf_2] Ionic Liquids with the Dissolved Gases H_2, He, N_2, CO, CO_2, or Kr Close to Infinite Dilution. *J. Chem. Eng. Data* **2020**, *65* (8), 4116−4129.
(73) Tomida, D.; Kenmochi, S.; Tsukada, T.; Qiao, K.; Yokoyama, C. Thermal Conductivities of Imidazolium-Based Ionic Liquid + CO_2 Mixtures. *Int. J. Thermophys.* **2010**, *31* (10), 1888−1895.
(74) Al-Barghouti, K. S.; Scurto, A. M. Thermal Conductivity of 1-Alkyl-3-methylimidazolium [Tf2N] Ionic Liquids and Compressed 1,1,1,2-Tetrafluoroethane (R-134a). *J. Chem. Eng. Data* **2022**, *67* (8), 1796−1809.
(75) Ren, W.; Scurto, A. M. Global Phase Behavior of Imidazolium Ionic Liquids and Compressed 1,1,1,2-Tetrafluoroethane (R-134a). *AIChE J.* **2009**, *55* (2), 486−493.
(76) Al-Barghouti, K. S.; Schmidt, H.; Eichberger, E.; Scurto, A. M.; Shiflett, M. B. A New Method to Combine High-Pressure Vapor Liquid Equilibrium and Thermophysical Property Measurements for Low-Volatility Liquids and a Gas. *J. Chem. Thermodyn.*, **2023**, In press.
(77) Lightfoot, E. N.; Bird, R. B.; Stewart, W. E. *Transport Phenomena*; John Wiley & Sons, Inc., 2006.
(78) Duncan, A. M. High-Pressure Viscosity of Biodiesel, Diesel, and Biodiesel-Diesel Blends: Experimental Data and Modeling. PhD Dissertation, University of Kansas, 2015.
(79) Ahosseini, A.; Scurto, A. M. Viscosity of imidazolium-based ionic liquids at elevated pressures: Cation and anion effects. *Int. J. Thermophys.* **2008**, *29* (4), 1222−1243.
(80) Morais, A. R. C.; Simoni, L. D.; Shiflett, M. B.; Scurto, A. M. Viscosity and Density of a Polyol Ester Lubricating Oil Saturated with Compressed Hydrofluoroolefin Refrigerants. *J. Chem. Eng. Data* **2020**, *65* (9), 4335−4346.
(81) NIST. *NIST Standard Reference Database 23: Reference Fluid Thermodynamic and Transport Properties-REFPROP, Version 10.0, National Institute of Standards and Technology, Standard Reference Data Program*: Gaithersburg, 2018.
(82) Healy, J. J.; deGroot, J. J.; Kestin, J. The Theory of the Transient Hot-Wire Method for Measuring Thermal Conductivity. *Phys. B+C* **1976**, *82* (2), 392−408.
(83) Assael, M. J.; Bogdanou, I.; Mylona, S. K.; Huber, M. L.; Perkins, R. A.; Vesovic, V. Reference Correlation of the Thermal Conductivity of n-Heptane from the Triple Point to 600 K and up to 250 MPa. *J. Phys. Chem. Ref. Data* **2013**, *42* (2), 023101.
(84) Assael, M. J.; Charitidou, E.; de Castro, C. A. N.; Wakeham, W. A. The Thermal Conductivity of n-Hexane, n-Heptane, and n-Decane by the Transient Hot-Wire Method. *Int. J. Thermophys.* **1987**, *8*, 663−670.
(85) Castro, C. A. N. d.; Calado, J. C. G.; Wakeham, W. A.; Dix, M. An apparatus to measure the thermal conductivity of liquids. *J. Phys. E Sci. Instrum.* **1976**, *9* (12), 1073−1080.
(86) Nagasaka, Y.; Nagashima, A. Precise measurements of the thermal conductivity of toluene and n-heptane by the absolute transient hot-wire method. *Ind. Eng. Chem. Fundam.* **1981**, *20* (3), 216−220.
(87) Qun-Fang, L.; Rui-Sen, L.; Dan-Yan, N.; Yu-Chun, H. Thermal Conductivities of Some Organic Solvents and Their Binary Mixtures. *J. Chem. Eng. Data* **1997**, *42* (5), 971−974.
(88) Menashe, J.; Wakeham, W. A. Absolute Measurements of the Thermal Conductivity of Liquids at Pressures up to 500 MPa. *Ber. Bunsenges. Phys. Chem.* **1981**, *85* (4), 340−347.

https://doi.org/10.1021/acs.iecr.3c03491
Ind. Eng. Chem. Res. 2024, 63, 1151−1169

(89) Tillner-Roth, R.; Yokozeki, A. An International Standard Equation of State for Difluoromethane (R-32) for Temperatures from the Triple Point at 136.34 K to 435 K and Pressures up to 70 MPa. *J. Phys. Chem. Ref. Data* **1997**, *26*, 1273−1328.
(90) Lemmon, E. W.; Jacobsen, R. T. A New Functional Form and New Fitting Techniques for Equations of State with Application to Pentafluoroethane (HFC-125). *J. Phys. Chem. Ref. Data* **2005**, *34* (1), 69−108.
(91) Mathias, P. M.; Klotz, H. C.; Prausnitz, J. M. Equation-of-State mixing rules for multicomponent mixtures: the problem of invariance. *Fluid Phase Equilib.* **1991**, *67*, 31−44.
(92) Boston, J. F.; Mathias, P. M. Phase Equilibria in a Third-Generation Process Simulator. *Proceedings of the 2nd International Conference on Phase Equilibria and Fluid Properties in the Chemical Process Industries*; Springer: West Berlin, 1980; pp 823−849.
(93) Valderrama, J. O.; Forero, L. A.; Rojas, R. E. Critical Properties and Normal Boiling Temperature of Ionic Liquids. Update and a New Consistency Test. *Ind. Eng. Chem. Res.* **2012**, *51* (22), 7838−7844.
(94) Valderrama, J. O.; Robles, P. A. Critical Properties, Normal Boiling Temperatures, and Acentric Factors of Fifty Ionic Liquids. *Ind. Eng. Chem. Res.* **2007**, *46* (4), 1338−1344.
(95) Tillner-Roth, R.; Baehr, H. D. An International Standard Formulation for the Thermodynamic Properties of 1,1,1,2-Tetrafluoroethane (HFC-134a) for Temperatures from 170 K to 455 K and Pressures up to 70 MPa. *J. Phys. Chem. Ref. Data* **1994**, *23*, 657−729.
(96) Makino, T.; Kanakubo, M.; Masuda, Y.; Umecky, T.; Suzuki, A. CO_2 absorption properties, densities, viscosities, and electrical conductivities of ethylimidazolium and 1-ethyl-3-methylimidazolium ionic liquids. *Fluid Phase Equilib.* **2014**, *362*, 300−306.
(97) Caqueret, V.; Berkalou, K.; Havet, J.-L.; Debacq, M.; Vitu, S. Density, Excess Molar Volume and Vapor-Liquid Equilibrium Measurements at 101.3 kPa for Binary Mixtures Containing Ethyl Acetate and a Branched Alkane: Experimental Data and Modeling. *Liquids* **2023**, *3* (2), 187−202.
(98) Adam, O. E.-A. A.; Awwad, A. M. Estimation of excess molar volumes and theoretical viscosities of binary mixtures of benzene + n-alkanes at 298.15 K. *Int. J. Ind. Chem.* **2016**, *7* (4), 391−400.
(99) Curras, M. R.; Mato, M. M.; Sanchez, P. B.; Garcia, J. Experimental densities of 2,2,2-trifluoroethanol with 1-butyl-3-methylimidazolium hexafluorophosphate at high pressures and modelling with PC-SAFT. *J. Chem. Thermodyn.* **2017**, *113*, 29−40.
(100) Anwar, N.; Riyazuddeen; Yasmeen, S. Corrigendum to "Volumetric, compressibility and viscosity studies of binary mixtures of [EMIM] [NTf2] with ethyl acetate/methanol at (298.15−323.15) K" [J. Mol. Liqs. 224 (2016) 189−200]. *J. Mol. Liq.* **2017**, *241*, 520−524.
(101) Bahadur, I.; Letcher, T. M.; Singh, S.; Redhi, G. G.; Venkatesu, P.; Ramjugernath, D. Excess molar volumes of binary mixtures (an ionic liquid+water): A review. *J. Chem. Thermodyn.* **2015**, *82*, 34−46.
(102) Meyer, C. W.; Morrison, G. Dipole moments of seven refrigerants. *J. Chem. Eng. Data* **1991**, *36* (4), 409−413.
(103) Gbur, A. M.; Johnson, P. Determination of dielectric properties of refrigerants. *ASHRAE Trans.* **2005**, *111*, 26−36.
(104) McGowan, J. C. Estimates of the Properties of Liquids. *J. Appl. Chem. Biotechnol.* **1978**, *28*, 599−607.
(105) Klähn, M.; Seduraman, A. What Determines CO_2 Solubility in Ionic Liquids? A Molecular Simulation Study. *J. Phys. Chem. B* **2015**, *119* (31), 10066−10078.
(106) Huang, X.; Margulis, C. J.; Li, Y.; Berne, B. J. Why Is the Partial Molar Volume of CO_2 so Small When Dissolved in a Room Temperature Ionic Liquid? Structure and Dynamics of CO_2 Dissolved in [Bmim] [PF_6]. *J. Am. Chem. Soc.* **2005**, *127* (50), 17842−17851.
(107) Zhang, Y.; Wang, X.; Yin, J. Viscosity of saturated mixtures of 1-hexyl-3-methyl-imidazolium bis(trifluoromethylsulfonyl)amide with R600a and R152a. *J. Chem. Thermodyn.* **2020**, *141*, 105970.
(108) May, E. F.; Moldover, M. R.; Schmidt, J. W. The Dielectric Permittivity of Saturated Liquid Carbon Dioxide and Propane Measured Using Cross Capacitors. *Int. J. Thermophys.* **2005**, *26* (3), 563−576.
(109) Powell, R. E.; Roseveare, W. E.; Eyring, H. Diffusion, Thermal Conductivity, and Viscous Flow of Liquids. *Ind. Eng. Chem. Res.* **1941**, *33* (4), 430−435.
(110) Wu, D. T. Prediction of viscosities of liquid mixtures by a group contribution method. *Fluid Phase Equilib.* **1986**, *30*, 149−156.
(111) Novak, L. T.; Chen, C.-C.; Song, Y. Segment-Based Eyring-NRTL Viscosity Model for Mixtures Containing Polymers. *Ind. Eng. Chem. Res.* **2004**, *43* (19), 6231−6237.
(112) Cao, W.; Fredenslund, A.; Rasmussen, P. Statistical thermodynamic model for viscosity of pure liquids and liquid mixtures. *Ind. Eng. Chem. Res.* **1992**, *31* (11), 2603−2619.
(113) Renon, H.; Prausnitz, J. M. Local compositions in thermodynamic excess functions for liquid mixtures. *AIChE J.* **1968**, *14* (1), 135−144.
(114) Huber, M. L.; Laesecke, A.; Perkins, R. A. Model for the Viscosity and Thermal Conductivity of Refrigerants, Including a New Correlation for the Viscosity of R134a. *Ind. Eng. Chem. Res.* **2003**, *42* (13), 3163−3178.
(115) Perkins, R. A.; Laesecke, A.; Howley, J.; Ramires, M. L. V.; Gurova, A. N.; Cusco, L. *Experimental Thermal Conductivity Values for the IUPAC Round Robin Sample of 1,1,1,2-Tetrafluoroethane (R134a)*; NISTIR, 6605, 2000.
(116) Fanning, J. T. *A Practical Treatise on Hydraulic and Water-Supply Engineering: Relating to the Hydrology, Hydrodynamics, and Practical Construction of Water-Works, in North America*; Van Nostrand: New York, 1877.
(117) Genereaux, R. P. Fluid-Flow Design Methods. *Ind. Eng. Chem. Res.* **1937**, *29* (4), 385−388.
(118) Sieder, E. N.; Tate, G. E. Heat Transfer and Pressure Drop of Liquids in Tubes. *Ind. Eng. Chem.* **1936**, *28* (12), 1429−1435.
(119) Bergman, T. L.; Lavine, A. S. *Fundamentals of Heat and Mass Transfer*; John Wiley & Sons, 2010.
(120) Tavousi, E.; Perera, N.; Flynn, D.; Hasan, R. Heat transfer and fluid flow characteristics of the passive method in double tube heat exchangers: A critical review. *Int. J. Thermofluids* **2023**, *17*, 100282.

https://doi.org/10.1021/acs.iecr.3c03491
Ind. Eng. Chem. Res. 2024, 63, 1151−1169